

AD\_\_\_\_\_

Award Number: W81XWH-11-1-0036

TITLE: Understanding the Effects of Cytotoxic Chemotherapeutics on the Innate Immune System

PRINCIPAL INVESTIGATOR: Elizabeth S. Nakasone

CONTRACTING ORGANIZATION: Cold Spring Harbor Laboratory  
Cold Spring Harbor, NY 11724

REPORT DATE: March 2012

TYPE OF REPORT: Annual Summary

PREPARED FOR: U.S. Army Medical Research and Materiel Command  
Fort Detrick, Maryland 21702-5012

DISTRIBUTION STATEMENT: Approved for Public Release;  
Distribution Unlimited

The views, opinions and/or findings contained in this report are those of the author(s) and should not be construed as an official Department of the Army position, policy or decision unless so designated by other documentation.

REPORT DOCUMENTATION PAGE				Form Approved OMB No. 0704-0188	
Public reporting burden for this collection of information is estimated to average 1 hour per response, including the time for reviewing instructions, searching existing data sources, gathering and maintaining the data needed, and completing and reviewing this collection of information. Send comments regarding this burden estimate or any other aspect of this collection of information, including suggestions for reducing this burden to Department of Defense, Washington Headquarters Services, Directorate for Information Operations and Reports (0704-0188), 1215 Jefferson Davis Highway, Suite 1204, Arlington, VA 22202-4302. Respondents should be aware that notwithstanding any other provision of law, no person shall be subject to any penalty for failing to comply with a collection of information if it does not display a currently valid OMB control number. <b>PLEASE DO NOT RETURN YOUR FORM TO THE ABOVE ADDRESS.</b>					
1. REPORT DATE March 2012		2. REPORT TYPE Annual Summary		3. DATES COVERED 1 January 2011 – 29 February 2012	
4. TITLE AND SUBTITLE  Understanding the Effects of Cytotoxic Chemotherapeutics on the Innate Immune System				5a. CONTRACT NUMBER	
				5b. GRANT NUMBER W81XWH-11-1-0036	
				5c. PROGRAM ELEMENT NUMBER	
6. AUTHOR(S)  Elizabeth S. Nakasone  E-Mail: nakasone@cshl.edu				5d. PROJECT NUMBER	
				5e. TASK NUMBER	
				5f. WORK UNIT NUMBER	
7. PERFORMING ORGANIZATION NAME(S) AND ADDRESS(ES)  Cold Spring Harbor Laboratory Cold Spring Harbor, NY 11724				8. PERFORMING ORGANIZATION REPORT NUMBER	
9. SPONSORING / MONITORING AGENCY NAME(S) AND ADDRESS(ES) U.S. Army Medical Research and Materiel Command Fort Detrick, Maryland 21702-5012				10. SPONSOR/MONITOR'S ACRONYM(S)	
				11. SPONSOR/MONITOR'S REPORT NUMBER(S)	
12. DISTRIBUTION / AVAILABILITY STATEMENT Approved for Public Release; Distribution Unlimited					
13. SUPPLEMENTARY NOTES					
14. ABSTRACT  In breast cancer, myeloid cells recruitment into tumors following radiation therapy and chemotherapy is frequently observed in pre-clinical models. We therefore sought to determine the significance of myeloid cell recruitment following chemotherapy treatment and their role in therapeutic resistance. Using intravital imaging of tumors in live mice, we observed that the tumors of the polyoma middle T antigen (PyMT) mouse model of luminal breast cancer show a stage-dependent sensitivity to treatment with doxorubicin. Doxorubicin treatment recruits CCR2+Gr1+7/4+CD11b+ immature myeloid cells with monocytic morphology. Inhibition of this recruitment via orthotopic transplantation of Ccr2+/+ cancer cells from PyMT mice into Ccr2-/- mice enhances the response to doxorubicin. Furthermore, changes in tumor vasculature and tumor grade accompany this improved response, indicating that CCR2 signaling may play important roles in tumor proliferation and differentiation, angiogenesis, in addition to therapeutic response. The data herein presented show that antagonism of CCR2 signaling in combination with cytotoxic chemotherapy treatment may be a potentially powerful therapeutic strategy for the treatment of breast cancer.					
15. SUBJECT TERMS Chemoresistance; breast cancer; chemokine; doxorubicin; intravital imaging; myeloid cell infiltration; tumor microenvironment					
16. SECURITY CLASSIFICATION OF:			17. LIMITATION OF ABSTRACT	18. NUMBER OF PAGES	19a. NAME OF RESPONSIBLE PERSON
a. REPORT	b. ABSTRACT	c. THIS PAGE			USAMRMC
U	U	U	UU	36	19b. TELEPHONE NUMBER (include area code)

## Table of Contents

Introduction .....	1
Body .....	1
Key Research Accomplishments .....	5
Reportable Outcomes .....	6
Conclusion .....	6
Appendices .....	9

## **I. INTRODUCTION**

Interactions between tumor cells and the immune system play a critical role in the progression and metastasis of many types of cancers. In breast tumors, the primary leukocyte population is the tumor-associated myeloid cell (O'Sullivan et al., 1994), which can promote tumor angiogenesis (Lin et al., 2006), intravasation and metastasis (Wyckoff et al., 2007), and contribute to therapeutic response (Ahn et al., 2010; DeNardo et al., 2011; Shree et al., 2011). Thus, therapeutic targeting of these tumor-associated macrophages – perhaps by depletion, inhibition of recruitment, re-polarization, or antagonism of pro-tumorigenic functions – may prove to be a potentially powerful means of treating breast cancer (Bingle et al., 2002; Luo et al., 2006).

The aims of this project are to understand how treatment of murine breast tumors with the cytotoxic chemotherapeutic doxorubicin affects the myeloid cell component of intact, solid tumors *in vivo*, and to determine how changes in this myeloid cell population following chemotherapy influence therapeutic response. Intravital imaging of tumors in live mice showed that the tumors of the polyoma middle T antigen (PyMT) mouse model of luminal breast cancer respond to doxorubicin by undergoing necrosis in drug-sensitive lesions. The presence of necrotic debris consequently results in the recruitment of CCR2<sup>+</sup>Gr1<sup>7/4</sup>CD11b<sup>+</sup> immature myeloid cells with monocytic morphology. Inhibition of this recruitment improves the response to doxorubicin indicating a role for these monocytic cells in therapeutic response. Changes in tumor vasculature and tumor grade accompany this improved response, indicating that CCR2 signaling may also have important effects on tumor angiogenesis and cancer cell differentiation and proliferation. The data herein presented show that antagonism of CCR2 signaling in combination with cytotoxic chemotherapy treatment may be a potentially powerful therapeutic strategy for the treatment of breast cancer.

## **II. SUMMARY OF TRAINING AND RESULTS**

### **Summary of Training**

#### ***Training Task 1a. Watson School of Biological Sciences (WSBS) required coursework.***

All primary coursework has been completed. The remaining coursework, including three post-graduate courses and four “Topics in Biology” courses have also been completed. The three post-graduate courses taken include attendance of the 2009 American Association for Cancer Research’s (AACR) Special Conference on Advances in Breast Cancer Research, Cold Spring Harbor Laboratory’s 2010 summer post-graduate course on Advanced Bacterial Genetics, and the AACR’s 2011 Translational Cancer Research for Basic Scientists Workshop. The four “Topics in Biology” courses taken are Evolution (2009), Statistics (2010), Immunology (2011), and Physical Biology of the Cell (2011).

#### ***Training Task 1b. Supplemental Coursework.***

Two supplemental courses were scheduled to be taken: the American Association of Immunologist’s Advanced Course in Immunology and the AACR’s Pathobiology of Cancer workshop. The former class was not taken, as Immunology was offered as a “Topics in Biology” course at CSHL. The second course was not taken, as it has not been offered during 2010 or 2011. The AACR’s Translational Cancer Research for Basic Scientists was taken in November 2011.

#### ***Training Task 1c. Teaching Responsibilities.***

The WSBS teaching requirement was fulfilled at the CSHL Dolan DNA Learning Center January through April 2009. Graduate students designed and executed lesson plans for two laboratories during the teaching rotation: DNA Extraction for middle school students and Restriction Digests for high school students. In addition to these teaching responsibilities, I mentored a second high school student from CSHL's Partners for the Future program during the 2010-2011 school year, and am mentoring a WSBS rotation student.

### ***Training Task 2. Meetings and Seminars.***

In 2011, I attended the inaugural The Biology of Cancer: Microenvironment, Therapeutics and Metastasis (2011) meeting at CSHL, and gave an oral presentation. In addition, I have given two In-House presentations at CSHL's Cancer Center In-House Seminar series, an oral presentation at CSHL's lab-wide Graduate Student Symposium, and presented a poster at CSHL's annual In-House Symposium (2011).

### **Summary of Results**

As the period of time between submission of the first year annual report (for the period covering January 1, 2011 to February 28, 2012) and the final report (for the period covering January 1 2011 to March 31, 2012) is only a month, there are no additional results to report. All of the aims proposed in the initial grant application have been addressed, as described below and the final report is therefore almost identical to the first year progress report. The results herein presented will be published on April 17, 2012 in *Cancer Cell* (doi:10.1016/j.ccr.2012.02.017).

The research aims of the grant application were:

Aim 1: Determine the effects of cytotoxic chemotherapy on the innate immune response;

Aim 2: Determine the importance of myeloid cell recruitment in tumor progression following chemotherapy.

Figures referred to in the following text are located in Appendix I. Refer to the attached proof for the *in press* manuscript, Nakasone *et al.* 2012 (Appendix II), for experimental details.

### ***Task 1. Determine the effects of cytotoxic chemotherapy on the innate immune response.***

#### ***Tasks 1a and 1b. Intravital microscopy of tumor-bearing mice and analysis of movies.***

To confirm the observation that myeloid cells are recruited into tumors following doxorubicin treatment, we performed intravital confocal microscopy of MMTV-PyMT;ACTB-EGFP;c-fms-EGFP triple transgenic mice. From the movies generated during these experiments, still image time series were created for each movie (Bitplane, Imaris). Each time series consisted of maximum intensity projections captured at one-hour intervals based on imaging time (Figure 1A, representative images from two still series). These time series were scored blindly for increases in myeloid cell infiltration into each field (i.e. increases in EGFP positivity over time). This analysis confirmed the observation made during our pilot experiments indicating that myeloid cells were being recruited following doxorubicin treatment. The results showed that 12 of 16 movies showed an increase in myeloid cell infiltration in doxorubicin-treated tumors, as compared to 3 of 16 movies for control tumors ( $p = 0.004$ , Fisher's exact test, Figure 1B). Furthermore, the highest degree of myeloid cell infiltration occurred in areas exhibiting a high degree of cell death. These results confirm previous findings by others that indicate a reactive recruitment of myeloid cells (primarily macrophages) following radiation therapy or chemotherapy (Ahn *et al.*, 2010; DeNardo *et al.*, 2011).

***Task 1c. Immunohistochemical analysis to determine populations of myeloid cells infiltrating the tumor tissue in doxorubicin treated and untreated mice.***

We identified CCL2 as the chemokine regulating myeloid cell recruitment after doxorubicin treatment (see ***Task 2a*** below). Mouse *Ccl2* (also known as monocyte chemoattractant protein-1, MCP-1) is a potent chemoattractant for monocytes (Tsui et al., 2007), and binds almost exclusively to the G<sub>i</sub>-protein-coupled receptor (GPCR) CCR2 (Deshmane et al., 2009). Thus, we used double label immunofluorescence staining for 7/4 (a marker of neutrophils and monocytes) and CCR2 on tumor tissues harvested from PBS- and doxorubicin-treated mice to identify and quantify the population of myeloid cells that infiltrate tumors after doxorubicin treatment. Double label immunostains were quantified based on positivity for one or both 7/4 and CCR2, as well as nuclear morphology. These stains showed that neutrophils almost always expressed 7/4 but not CCR2, while monocytes were nearly always double positive for 7/4 and CCR2 (Figure 2AA).

Quantification of double-label immunostains (104 fields from doxorubicin-treated mice, 113 fields from control mice) showed a significant increase in the total number of 7/4<sup>+</sup> immune cells per field (regardless of nuclear morphology or staining for CCR2) in the tumors of doxorubicin-treated mice, as compared to those of PBS-treated mice. Furthermore, nearly all of these infiltrating 7/4<sup>+</sup> were CCR2<sup>+</sup> cells exhibiting a monocytic nuclear morphology. Although a small number of 7/4<sup>+</sup> cells exhibiting neutrophilic morphology and positive for CCR2 were detected, there was no difference in the numbers of this cell population between tumors from doxorubicin- as compared to PBS-treated mice. This trend was also true of cells that expressed CCR2 but were negative for the 7/4 antigen. Additionally, the tumors of doxorubicin-treated mice showed a significant decrease in the number of cells that expressed the 7/4 antigen but were negative for CCR2, regardless of whether they exhibited a monocytic or neutrophilic morphology (Figure 2B).

***Task 1d. Confirmation of 7/4<sup>+</sup> immature myeloid cell recruitment by flow cytometry.***

We used flow cytometric analyses of tumors harvested from PBS- or doxorubicin-treated mice to confirm the recruitment of 7/4<sup>+</sup> monocytes into tumors. We combined staining of 7/4 with staining of Gr1 (another marker of neutrophils and monocytes, as well as immature myeloid cells) and the pan-myeloid cell marker CD11b. We also stained for F4/80, a marker of macrophages, to determine whether there was a change in this population as well.

Flow cytometric analyses were based on 11 mice (1 tumor per mouse) treated with PBS, and 10 mice (1 tumor per mouse) treated with doxorubicin. We confirmed the increase in numbers of immature myeloid cells triple-positive for Gr1, 7/4, and CD11b. In contrast, we observed no difference in the total number of CD11b<sup>+</sup> nor the F4/80<sup>+</sup>CD11b<sup>+</sup> double-positive immune cell populations by flow cytometry in the tumors of doxorubicin-treated mice, as compared to those of PBS-treated controls (Figure 3).

***Task 2a. Identification of CCL2 as the chemokine mediating myeloid cell recruitment.***

We previously identified CCL2 as the candidate chemokine regulating myeloid cell recruitment into tumors following doxorubicin treatment using spotted antibody arrays for cytokines and chemokines (R&D Systems, Figure 4A). There was a strong trend for increased expression of CCL2 in the tumors of doxorubicin-treated mice, as compared to those of PBS-treated control mice (Figure 4B). The results did not reach statistical significance, most likely reflecting the heterogeneity of MMTV-PyMT tumor responses to doxorubicin and the difficulties of detecting chemokines in whole tumor lysate.

***Task 2b. Determine the (short-term) effects of inhibiting the CCL2/CCR2 axis on myeloid cell recruitment and host response to chemotherapy.***

As it has recently been shown that CCL2 recruits monocytes to primary murine breast

tumors as well as metastatic sites (Qian et al., 2011), and stromal expression of CCL2 in human breast cancers is associated with both macrophage infiltration and decreased relapse-free survival (Fujimoto et al., 2009), we predicted that inhibition of CCL2/CCR2 signaling would enhance the response to doxorubicin treatment. Because the receptor for CCL2 (CCR2) recognizes other chemokines that may compensate for CCL2 depletion, we used a CCR2 antagonist to inhibit signaling through CCL2 activation. We tested the small molecule inhibitor RS 504393 (Roche/Iconix, Higgins et al., 2007), which has been previously used successfully to inhibit monocyte recruitment in infection and autoimmune models (Yang et al., 2009; Yang et al., 2010).

MMTV-PyMT tumor-bearing mice were pre-treated with either DMSO (vehicle) or RS 504393 every 12 hours beginning three days before doxorubicin (or PBS) treatment and continuing until just before euthanization. Tumor measurements were taken at the start treatment with vehicle or the inhibitor, and on days 0, 1, and 2 of doxorubicin or PBS treatment. Ultrasound (Vevo 770, VisualSonics) was performed on 2-3 tumors per mouse on days -3, 0, and 2 following doxorubicin treatment to determine whether there were any inhibitor-related changes in tumor necrosis and cysts. Flow cytometric analyses for 7/4, F4/80, and Gr1 were performed on a single tumor from each mouse to determine the effects of RS 504393 on myeloid cell recruitment. In addition, we imaged two mice treated with the inhibitor plus doxorubicin and two mice treated with the inhibitor plus PBS.

The tumor response in mice treated with the inhibitor showed the same responses to doxorubicin (and PBS) as vehicle treated tumors (Figure 5A,  $n = 9$  mice for vehicle + PBS,  $n = 10$  mice for all other groups,  $p$ -values are not significant at all time points using a Student's  $t$ -test when vehicle + PBS is compared to inhibitor + PBS or vehicle + doxorubicin is compared to inhibitor + doxorubicin). Furthermore, ultrasound revealed no differences in necrosis or cyst formation between tumors of vehicle-treated and inhibitor-treated mice receiving doxorubicin (data not shown). Flow cytometric analyses of vehicle-treated controls only showed a trend toward an increase in the F4/80<sup>+</sup>CD11b<sup>+</sup> population, as well as a decrease in the 7/4<sup>+</sup>CD11b<sup>+</sup> and Gr1<sup>+</sup>CD11b<sup>+</sup> populations in the doxorubicin-treated tumors of vehicle treated mice (Figure 5B,  $n = 3$  mice per group with 1 tumor per mouse). These results are opposite to those obtained from mice treated with doxorubicin or PBS alone (see Figure 3B). Imaging showed cancer cell and stromal cell death in the tumors of PBS-treated mice. The cell death in tumors of both PBS- and doxorubicin-treated mice that also received the inhibitor was accompanied by a high degree of myeloid cell infiltration (Figure 5C), and a high degree of myeloid cell death was also seen in the tumors of doxorubicin-treated mice that showed little or no cancer cell death. We speculate that the vehicle (DMSO) had a direct effect on the mice, as mice receiving vehicle alone showed signs of irritation, including sensitivity to touch. Furthermore, we have no data supporting that RS 504393 inhibited CCR2 at the dose and schedule used.

***Task 2b – Amended. Determine the (short-term) effects of inhibiting the CCL2/CCR2 axis on myeloid cell recruitment and host response to chemotherapy.***

Because CCR2 is expressed primarily in the stromal compartment (i.e. immune cells) we predicted that using a transplantation model in which  $Ccr2^{+/+}$  wildtype cancer cells transplanted into  $Ccr2^{-/-}$  hosts would recapitulate inhibition of myeloid cell recruitment. Primary cancer cells were harvested from the tumors of MMTV-PyMT (C57BL/6) wildtype for  $Ccr2$  and orthotopically transplanted into syngeneic  $Ccr2^{+/+}$  or  $Ccr2^{-/-}$  hosts. We first characterized this model to that ensure loss of stromal CCR2 expression did not produce any major effects on tumor growth that would hinder interpretation of any future results. We observed no differences in tumor take or tumor growth rate between wildtype and  $Ccr2^{-/-}$  hosts following cancer cell transplantation (Figures 6A and 6B,  $n = 17$  mice per treatment, log-rank score for survival curve, Student's  $t$ -test for growth curve). Furthermore, we could confirm with flow cytometric analyses that with acute doxorubicin treatment (48 hrs), loss of stromal CCR2 expression prevented recruitment of

immature myeloid cells (Figure 6C, n = 11 mice per treatment, 1 tumor per mouse, Student's t-test).

We performed various histochemical analyses on tissues from *Ccr2*<sup>+/+</sup> and *Ccr2*<sup>-/-</sup> hosts to characterize the effects of losing stromal CCR2 expression on chemotherapy response. Hematoxylin and eosin (HE) staining on tumors harvested 48 hrs after doxorubicin treatment showed that the tumors of *Ccr2*<sup>-/-</sup> hosts were far more cystic with decreased cellularity as compared to tumors removed from wildtype hosts (Figure 7). We also looked at changes in vascular phenotype using lectin staining, as monocytes and macrophages promote tumor angiogenesis (Dirkx et al., 2006). We assessed vascular permeability using lectin staining for *Lycopersicon esculentum* (tomato) lectin, which labels all functional vasculature and *Ricinus communis* agglutinin I, which labels areas of increased vascular leakiness (Thurston et al., 1996). Analyses of these stains showed that the density of functional vasculature (as determined by tomato lectin staining) was higher in the tumors of *Ccr2*<sup>-/-</sup> hosts, while there was no change in the density of leaky vasculature, as determined by *Ricinus communis* agglutinin I staining. The net result of this change is a significant reduction in leaky tumor vasculature (Figure 8, n = 6 mice per genotype with 2 tumors per mouse, 48 fields for *Ccr2*<sup>+/+</sup> hosts and 46 fields for *Ccr2*<sup>-/-</sup> hosts).

This change is indicative of vascular normalization, which has been proposed as a model for anti-angiogenic cancer therapy (Jain et al., 2001). This vascular phenotype may be an indirect effect resulting from inhibiting myeloid cell recruitment into tumors. Tumor-associated macrophages and other tumor-infiltrating myeloid cells produce a variety of factors (including VEGF and matrix metalloproteinases) that promote tumor angiogenesis (Murdoch et al., 2008). Blockade of tumor angiogenesis via antibody-mediated neutralization of VEGF has been shown to induce tumor normalization and improve chemotherapeutic response (Tong et al., 2004; Vosseler et al., 2005). Given the effects we observe in our transplantation model, CCL2/CCR2 antagonism may represent another approach to targeting tumor angiogenesis. However, more work is needed to determine the exact mechanism regulating the change in vascular normalization, and whether this is important for the response to doxorubicin.

**Task 2c. Determine the long-term effects of inhibiting the CCL2/CCR2 axis on myeloid cell recruitment and host response to chemotherapy.**

Tumor-bearing *Ccr2*<sup>+/+</sup> and *Ccr2*<sup>-/-</sup> hosts were placed on a long-term doxorubicin regimen consisting of once weekly treatments for three weeks with follow-up (n = 8 tumors per genotype, 1 tumor per mouse). As expected, *Ccr2*<sup>-/-</sup> hosts responded better to doxorubicin than wildtype hosts (Figure 9, Student's t-test at each time point). These results are in line with those reported by other groups that have shown increased macrophage infiltration into MMTV-PyMT tumors after chemotherapy, and that inhibition of this recruitment enhances therapeutic response (DeNardo et al., 2011; Shree et al., 2011).

We performed hematoxylin and eosin staining to begin to understand how losing CCR2 expression in the stromal compartment influences the long-term response to doxorubicin. These histochemical analyses show that *Ccr2*<sup>-/-</sup> mice 6 weeks after treatment (4 weeks after the last dose) showed a much lower tumor grade as compared to those harvested from wildtype mice at the same time point (Figure 10, n = 1 low-grade and 11 high-grade tumors from *Ccr2*<sup>+/+</sup> hosts, n = 10 low-grade and 5 high-grade tumors in *Ccr2*<sup>-/-</sup> hosts, p = 0.005, Fisher's exact test).

These phenotypic changes imply that the cues present in the microenvironment are altered in *Ccr2*<sup>-/-</sup> hosts, and that cancer cells are responding to these changes. There is some evidence implicating CCL2 expression in promoting both cancer cell proliferation and motility (Valković et al., 1998; Dwyer et al., 2007; Nam et al., 2006; Loberg et al., 2006). However, there is still much work to be done to determine how this phenotypic change is occurring and the functional importance of this change on survival and response to adjuvant therapies.

### **III. KEY RESEARCH ACCOMPLISHMENTS**

- Treatment of MMTV-PyMT tumor-bearing mice with doxorubicin results in a reactive recruitment of myeloid cells into tumors
- Post-doxorubicin treatment recruitment of myeloid cells is dependent on CCL2/CCR2 signaling
- Inhibiting CCL2/CCR2 signaling improves the response to doxorubicin
- Tumors of *Ccr2*<sup>-/-</sup> hosts exhibit a low histopathological grade compared to the tumors of wildtype hosts
- Tumors of *Ccr2*<sup>-/-</sup> hosts show an increased vascular volume that is less leaky than the vasculature of tumors of wildtype hosts

### **IV. REPORTABLE OUTCOMES**

**Manuscripts, abstracts, and publications produced as a result of this funded research:**

1. Nakasone ES, Askautrud HA, Qiu J, Werb Z, Egeblad M. Understanding the effects of cytotoxic chemotherapeutics on the innate immune system. *The Biology of Cancer: Microenvironment, Therapeutics & Metastasis*. April 26-30, 2011.
2. Nakasone ES, Askautrud HA, Kees T, Qiu J, Egeblad M. Recruitment of myeloid cells through CCL2/CCR2 signaling promotes chemoresistance. *CSHL In-House Symposium XXV*. November 21-22, 2011.
3. Nakasone ES,\* Askautrud HA,\* Kees T, Park J-H, Plaks V, Ewald AJ, Fein M, Rasch MG, Tan Y-X, Qiu J, Park J, Sinha P, Bissell MJ, Frengen E, Werb Z, Egeblad M. 2012. Imaging tumor-stroma interactions during chemotherapy reveals contributions of the microenvironment to resistance. *Cancer Cell*. 2012. doi:10.1016/j.ccr.2012.02.017

#### **Degrees obtained:**

Ph.D. from the Watson School of Biological Sciences: Elizabeth Nakasone (P.I.) completed all of her Ph.D. requirements in March 2012.

### **V. CONCLUSIONS**

Treatment of mammary tumors with the cytotoxic chemotherapeutic doxorubicin alters the tumor-associated inflammatory microenvironment by inducing a reactive recruitment of immature myeloid cells via a stromal CCL2/CCR2 signaling axis. The increased presence of these myeloid cells promotes chemoresistance, and blockade of this signaling pathway delays host relapse and improves overall therapeutic response.

CCL2/CCR2 blockade results in several phenotypic changes in tumor pathology, including tumor grade and vascular organization, implying broader effects than just those indirectly resulting from the recruitment of tumor-promoting myeloid cells. While further work is needed to mechanistically untangle *in vivo* the effects of recruiting monocytes cells into tumors and the role of CCL2/CCR2 signaling in breast cancer epithelial cell proliferation and tumor angiogenesis, it is apparent that targeting CCL2 or CCR2 in combination with chemotherapeutic treatment is a potentially powerful therapeutic strategy.

### **VI. REFERENCES**

Ahn, G.-O., Tseng, D., Liao, C.-H., Dorie, M.J., Czechowicz, A., and Brown, J.M. (2010).

- Inhibition of Mac-1 (CD11b/CD18) enhances tumor response to radiation by reducing myeloid cell recruitment. *Proc. Natl. Acad. Sci. U.S.A.* 107, 8363–8368.
- Bingle, L., Brown, N.J., and Lewis, C.E. (2002). The role of tumour-associated macrophages in tumour progression: implications for new anticancer therapies. *J. Pathol.* 196, 254–265.
- DeNardo, D.G., Barreto, J.B., Andreu, P., Vaszquez, L., Tawfik, D., Kolhatkar, N., and Coussens, L.M. (2009). CD4(+) T cells regulate pulmonary metastasis of mammary carcinomas by enhancing protumor properties of macrophages. *Cancer Cell* 16, 91–102.
- DeNardo, D.G., Brennan, D.J., Rexhepaj, E., Ruffell, B., Shiao, S.L., Madden, S.F., Gallagher, W.M., Wadhwani, N., Keil, S.D., Junaid, S.A., et al. (2011). Leukocyte Complexity Predicts Breast Cancer Survival and Functionally Regulates Response to Chemotherapy. *Cancer Discov* 1, 54–67.
- Deshmane, S.L., Kremlev, S., Amini, S., and Sawaya, B.E. (2009). Monocyte chemoattractant protein-1 (MCP-1): an overview. *J. Interferon Cytokine Res.* 29, 313–326.
- Dirkx, A.E.M., Oude Egbrink, M.G.A., Wagstaff, J., and Griffioen, A.W. (2006). Monocyte/macrophage infiltration in tumors: modulators of angiogenesis. *J. Leukoc. Biol.* 80, 1183–1196.
- Dwyer, R.M., Potter-Beirne, S.M., Harrington, K.A., Lowery, A.J., Hennessy, E., Murphy, J.M., Barry, F.P., O'Brien, T., and Kerin, M.J. (2007). Monocyte chemotactic protein-1 secreted by primary breast tumors stimulates migration of mesenchymal stem cells. *Clin. Cancer Res.* 13, 5020–5027.
- Fujimoto, H., Sangai, T., Ishii, G., Ikehara, A., Nagashima, T., Miyazaki, M., and Ochiai, A. (2009). Stromal MCP-1 in mammary tumors induces tumor-associated macrophage infiltration and contributes to tumor progression. *Int J Cancer* 125, 1276–1284.
- Higgins, P.J., Schwartz, C.E., and Nicolas, J.-M. (2007). Small molecule CCR2 antagonists. In *Chemokine Biology — Basic Research and Clinical Application*, (Birkhauser), pp. 115–123.
- Jain, R.K. (2001). Normalizing tumor vasculature with anti-angiogenic therapy: a new paradigm for combination therapy. *Nat. Med.* 7, 987–989.
- Lin, E.Y., Li, J.-F., Gnatovskiy, L., Deng, Y., Zhu, L., Grzesik, D.A., Qian, H., Xue, X.-N., and Pollard, J.W. (2006). Macrophages regulate the angiogenic switch in a mouse model of breast cancer. *Cancer Res* 66, 11238–11246.
- Loberg, R.D., Day, L.L., Harwood, J., Ying, C., St John, L.N., Giles, R., Neeley, C.K., and Pienta, K.J. (2006). CCL2 is a potent regulator of prostate cancer cell migration and proliferation. *Neoplasia* 8, 578–586.
- Luo, Y., Zhou, H., Krueger, J., Kaplan, C., Lee, S.-H., Dolman, C., Markowitz, D., Wu, W., Liu, C., Reisfeld, R.A., et al. (2006). Targeting tumor-associated macrophages as a novel strategy against breast cancer. *J. Clin. Invest.* 116, 2132–2141.
- Murdoch, C., Muthana, M., Coffelt, S.B., and Lewis, C.E. (2008). The role of myeloid cells in the promotion of tumour angiogenesis. *Nat. Rev. Cancer* 8, 618–631.
- Nam, J.-S., Kang, M.-J., Suchar, A.M., Shimamura, T., Kohn, E.A., Michalowska, A.M., Jordan, V.C., Hirohashi, S., and Wakefield, L.M. (2006). Chemokine (C-C motif) ligand 2 mediates the prometastatic effect of dysadherin in human breast cancer cells. *Cancer Res* 66, 7176–7184.
- O'Sullivan, C., and Lewis, C.E. (1994). Tumour-associated leucocytes: friends or foes in breast carcinoma. *J. Pathol.* 172, 229–235.
- Qian, B.-Z., Li, J., Zhang, H., Kitamura, T., Zhang, J., Campion, L.R., Kaiser, E.A., Snyder, L.A., and Pollard, J.W. (2011). CCL2 recruits inflammatory monocytes to facilitate breast-tumour metastasis. *Nature*.
- Shree, T., Olson, O.C., Elie, B.T., Kester, J.C., Garfall, A.L., Simpson, K., Bell-McGuinn, K.M., Zabor, E.C., Brogi, E., and Joyce, J.A. (2011). Macrophages and cathepsin proteases blunt chemotherapeutic response in breast cancer. *Genes Dev.* 25, 2465–2479.

- Thurston, G., Baluk, P., Hirata, A., and McDonald, D.M. (1996). Permeability-related changes revealed at endothelial cell borders in inflamed venules by lectin binding. *Am. J. Physiol.* 271, H2547–62.
- Tong, R.T., Boucher, Y., Kozin, S.V., Winkler, F., Hicklin, D.J., and Jain, R.K. (2004). Vascular normalization by vascular endothelial growth factor receptor 2 blockade induces a pressure gradient across the vasculature and improves drug penetration in tumors. *Cancer Res* 64, 3731–3736.
- Tsui, P., Das, A., Whitaker, B., Tornetta, M., Stowell, N., Kesavan, P., Kaiser, E., Lacy, E.R., Yan, L., Snyder, L.A., et al. (2007). Generation, characterization and biological activity of CCL2 (MCP-1/JE) and CCL12 (MCP-5) specific antibodies. *Hum Antibodies* 16, 117–125.
- Valković, T., Lucin, K., Krstulja, M., Dobi-Babić, R., and Jonjić, N. (1998). Expression of monocyte chemotactic protein-1 in human invasive ductal breast cancer. *Pathol. Res. Pract.* 194, 335–340.
- Vosseler, S., Mirancea, N., Bohlen, P., Mueller, M.M., and Fusenig, N.E. (2005). Angiogenesis inhibition by vascular endothelial growth factor receptor-2 blockade reduces stromal matrix metalloproteinase expression, normalizes stromal tissue, and reverts epithelial tumor phenotype in surface heterotransplants. *Cancer Res* 65, 1294–1305.
- Wyckoff, J.B., Wang, Y., Lin, E.Y., Li, J.-F., Goswami, S., Stanley, E.R., Segall, J.E., Pollard, J.W., and Condeelis, J. (2007). Direct visualization of macrophage-assisted tumor cell intravasation in mammary tumors. *Cancer Res* 67, 2649–2656.
- Yang, D., Tong, L., Wang, D., Wang, Y., Wang, X., and Bai, C. (2010). Roles of CC chemokine receptors (CCRs) on lipopolysaccharide-induced acute lung injury. *Respir Physiol Neurobiol* 170, 253–259.
- Yang, S.J., IglayReger, H.B., Kadouh, H.C., and Bodary, P.F. (2009). Inhibition of the chemokine (C-C motif) ligand 2/chemokine (C-C motif) receptor 2 pathway attenuates hyperglycaemia and inflammation in a mouse model of hepatic steatosis and lipotrophy. *Diabetologia* 52, 972–981.

## VII. APPENDICES

### I. Figures

**Figure 1. Myeloid cells are recruited to tumors after doxorubicin treatment.** (A) Representative images of early carcinoma lesions imaged for 40 hours. Time indicates hh:mm post-doxorubicin treatment or matched imaging time (control). (B) Quantification of myeloid cell infiltration into tumors following doxorubicin treatment.

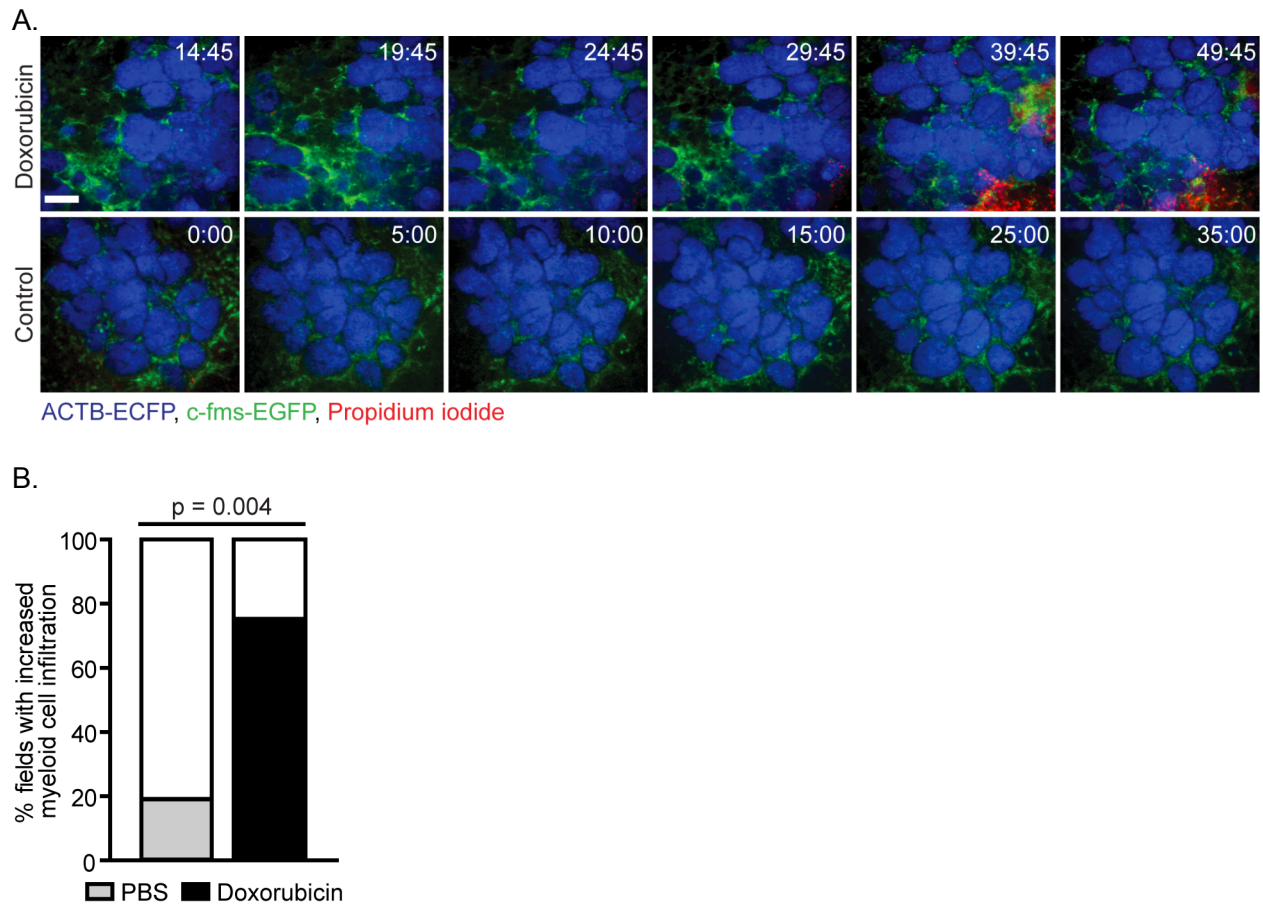


**Figure 2. CCL2 expression results in the recruitment of immature myeloid cells expressing CCR2<sup>+</sup> and exhibiting a monocytic nuclear phenotype.** (A) Representative photomicrograph of 7/4 and CCR2 double label immunostaining patterns for neutrophils and monocytes. Neutrophilic cells almost exclusive express 7/4 without CCR2 staining, while monocytic cells are almost always double positive for 7/4 and CCR2. Scale = 10  $\mu$ m. (B) Quantification of 7/4 and CCR2 double label immunostains. P-values are based on Student's t-test. Error is depicted as mean  $\pm$  SEM.

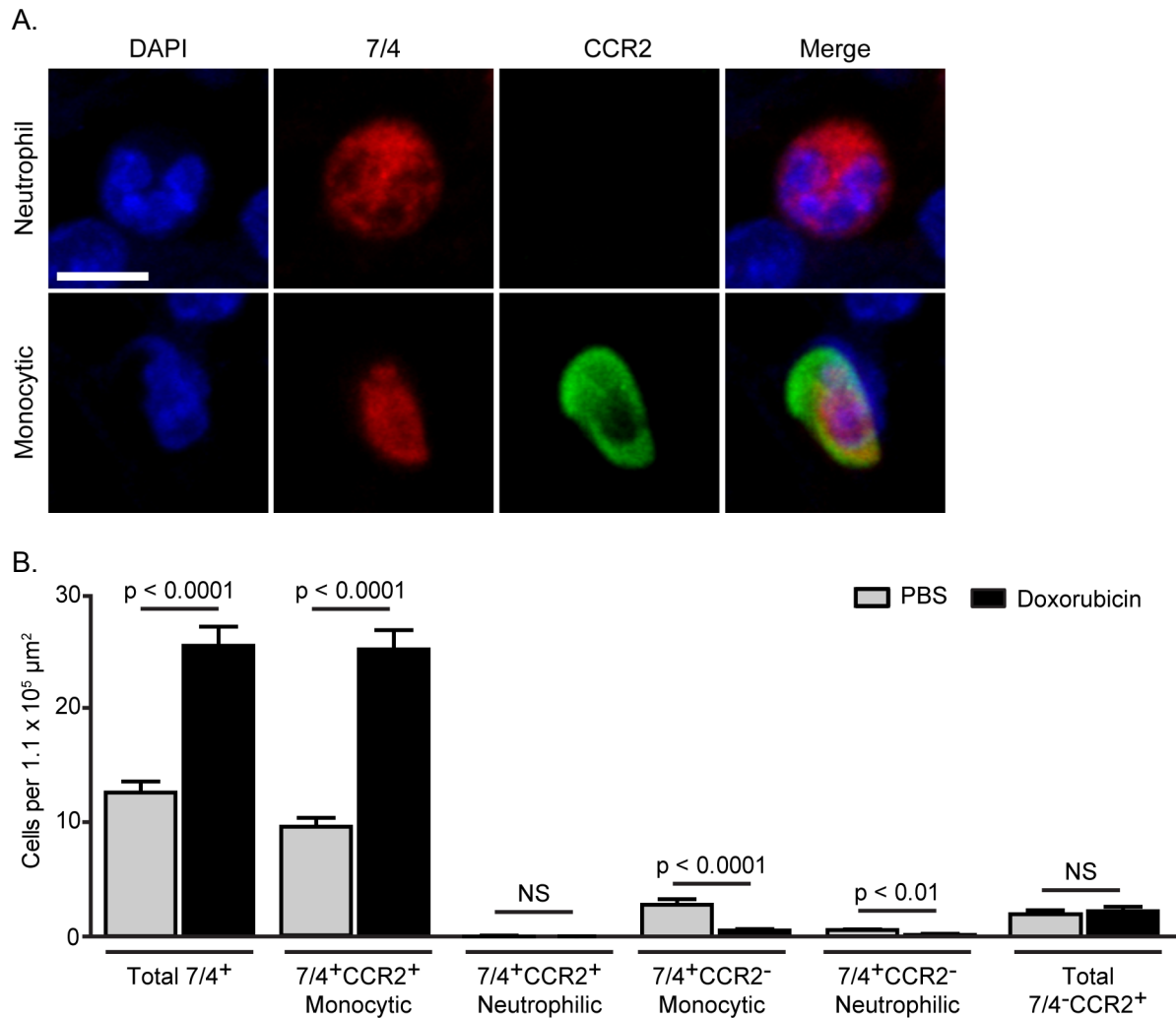
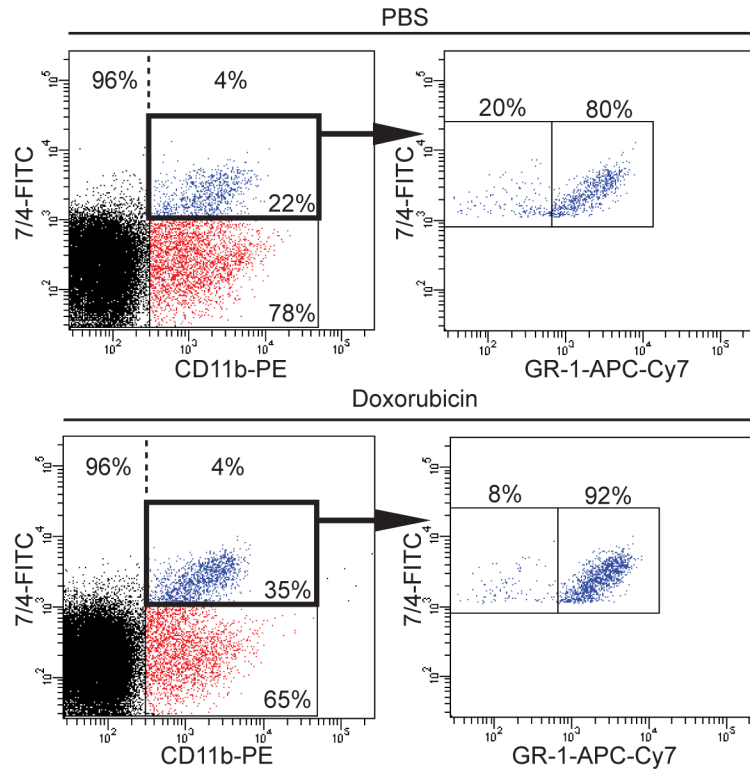


**Figure 3. Flow cytometric analyses confirm the recruitment of immature myeloid cells following doxorubicin treatment.** (A) Representative FACS plots for CD11b, Gr1, and 7/4 staining. The total cellular tumor population was first gated on CD11b (4% for both treatments in this plot). CD11b populations were then divided into two populations based on 7/4 expression ( $7/4^{\text{high}}$  and  $7/4^{\text{low}}$ ). Gr1 expression was then examined in the  $7/4^{\text{high}}$  population (again divided into two populations,  $\text{Gr1}^{\text{high}}$  and  $\text{Gr1}^{\text{low}}$ ). (B) Quantification of flow cytometric experiments. P-values are based on Student's t-test. Error is depicted as mean  $\pm$  SEM.

A.



B.

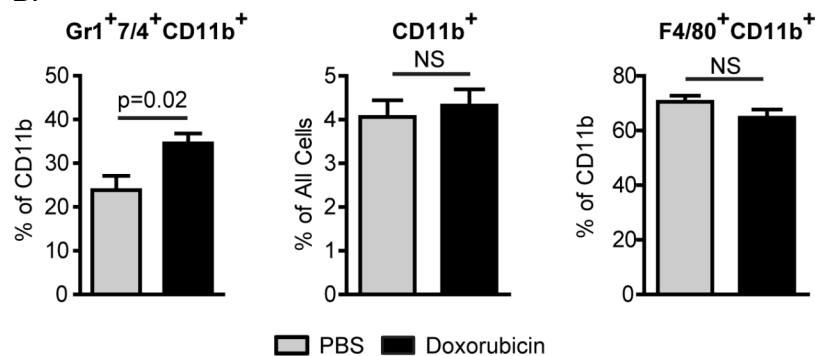


**Figure 4. The chemokine CCL2 is upregulated following doxorubicin treatment.** (A) Truncated cytokine array showing upregulation of CCL2 following doxorubicin treatment. Each column represents a single tumor (each tumor is from a different mouse). (B) ELISA also shows upregulation of CCL2 following doxorubicin treatment. Each dot represents a single tumor from a different mouse (n = 12 for each treatment). P = not significant, Student's t-test.

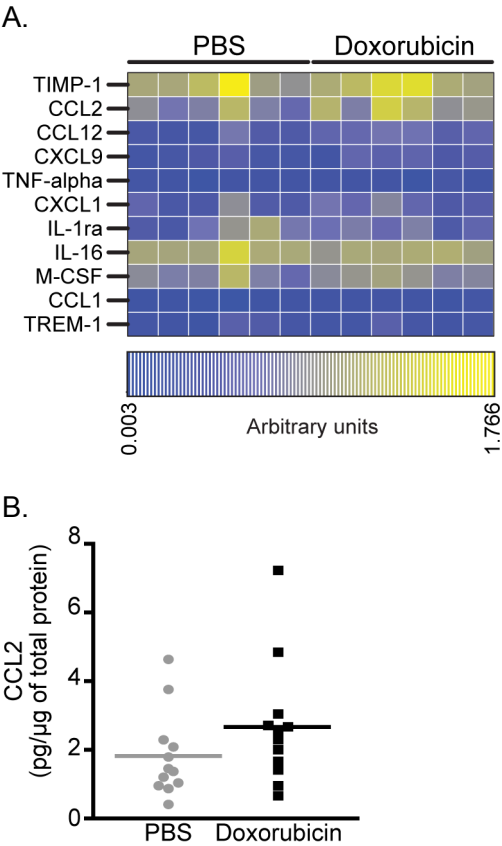


**Figure 5. Small-molecule inhibition of CCR2 with RS 504393.** (A) Acute response to treatment with the CCR2 inhibitor (CCR2i) RS 504393. (B) Quantification of flow cytometric data from control mice from CCR2i experiments. These results show trends toward the opposite of those obtained from mice treated with PBS or doxorubicin alone. (C) Representative images of intravital imaging experiments of CCR2i-treated mice. The movies obtained from these experiments are quite different from those obtained from untreated or doxorubicin-treated mice, indicating potential off-target effects of either the vehicle (DMSO) or the inhibitor. P-values are based on Student's t-test at each time point. Error is depicted as mean  $\pm$  SEM. Scale = 100  $\mu$ m.

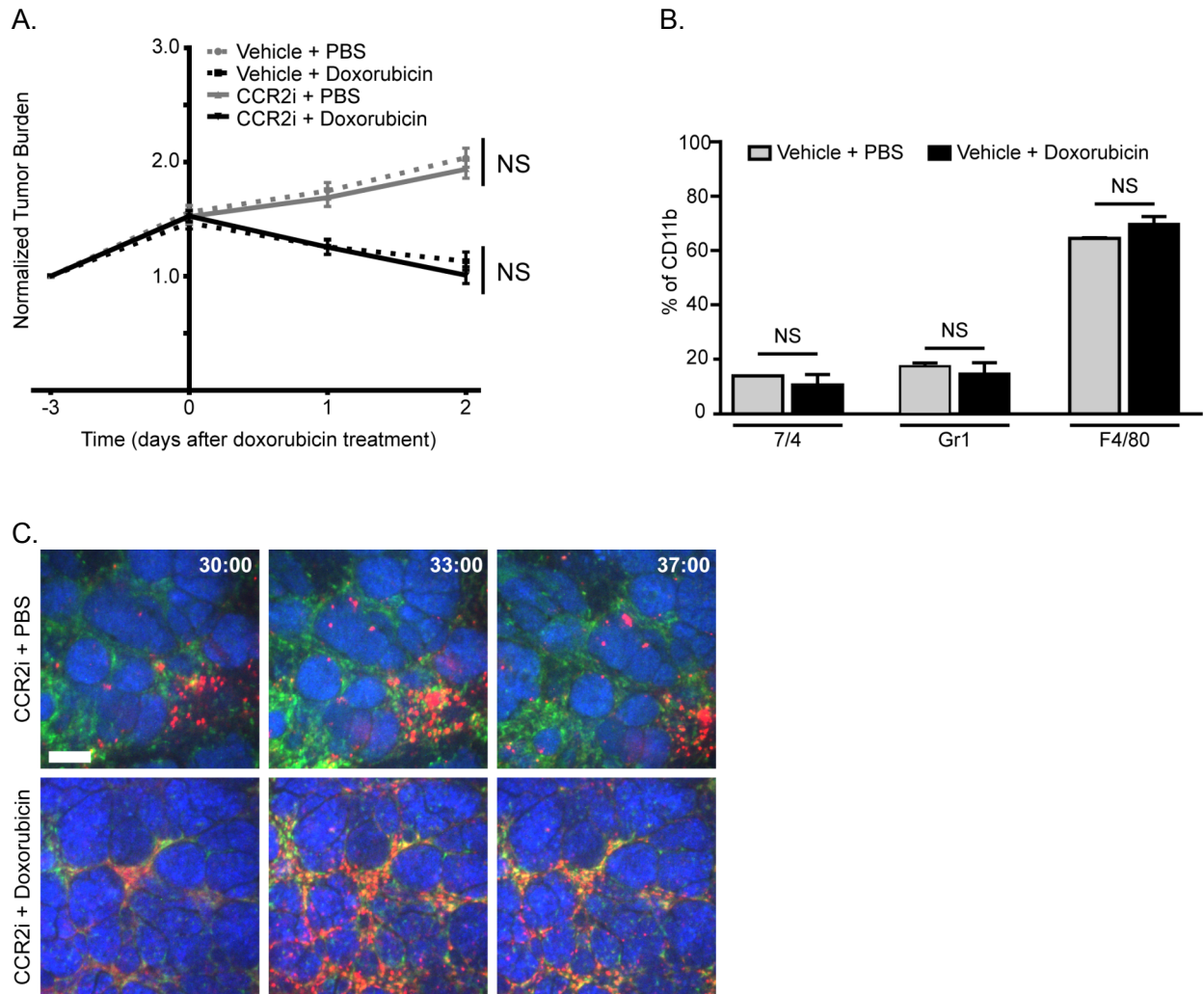


**Figure 6. Transplantation of *Ccr2*<sup>+/+</sup> cancer cells into *Ccr2*<sup>-/-</sup> hosts does not affect tumor take or tumor growth and inhibits the recruitment of immature myeloid cells.** (A) Kaplan-Meier curve of tumor incidence in *Ccr2*<sup>+/+</sup> or *Ccr2*<sup>-/-</sup> hosts transplanted with *Ccr2*<sup>+/+</sup> MMTV-PyMT cancer cells shows no difference in tumor take between hosts. (B) Tumor growth curve shows loss of stromal CCR2 expression has no effect on tumor growth. (C) Treatment of tumor-bearing transplant mice shows that loss of stromal CCR2 expression inhibits the recruitment of immature myeloid cells into tumors following doxorubicin treatment. P-values are based on Student's t-test at each time point. Error is depicted as mean ± SEM.

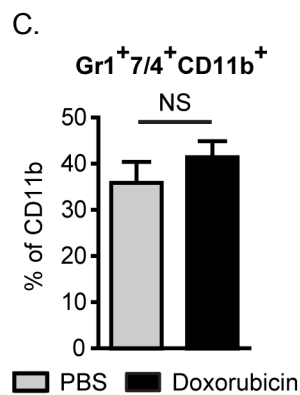
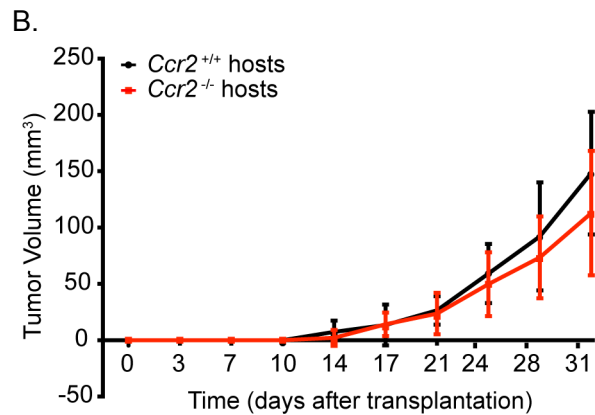
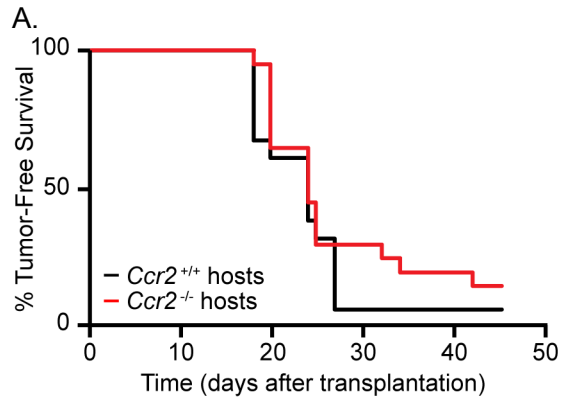


**Figure 7. Loss of stromal CCR2 expression alters the tumor phenotype following acute doxorubicin treatment.** Tumors of *Ccr2*<sup>-/-</sup> hosts are more cystic and have fewer cells as compared to wildtype hosts, 48 hrs after doxorubicin treatment. Scale = 100  $\mu$ m.

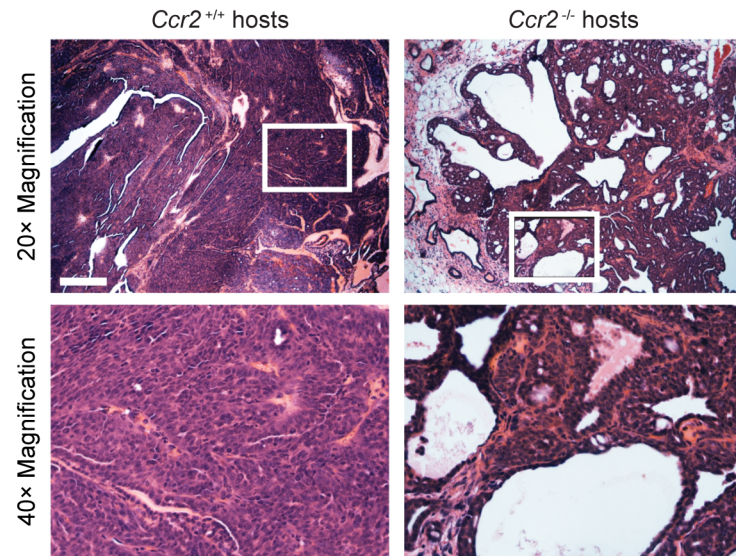
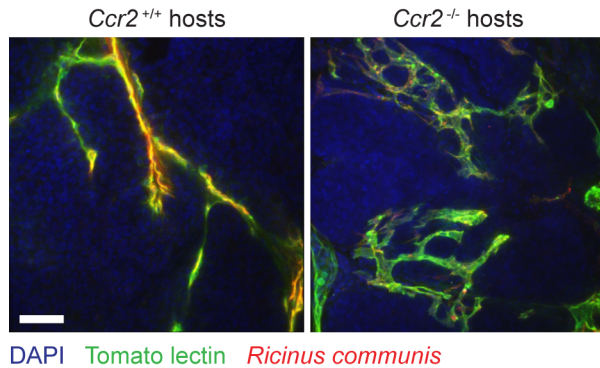
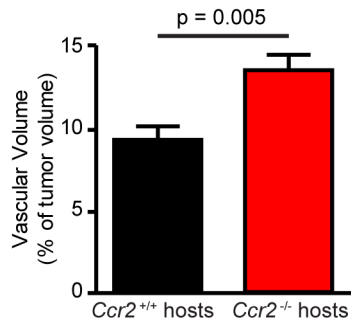


**Figure 8. Loss of stromal CCR2 expression alters the tumor vasculature.** (A) Representative images of lectin stains. Scale = 100  $\mu$ m. (B) Quantification of vascular (tomato lectin) volume. (C) Quantification of leaky vascular volume (*Ricinus communis*). (D) Quantification of the percentage of the total tumor volume that is leaky. P-values based on Student's t-test. Error depicted as mean  $\pm$  SEM.

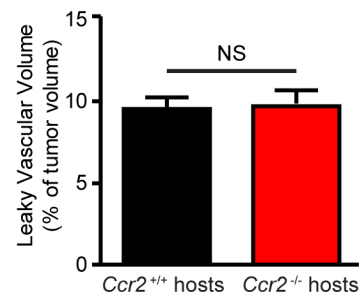
A.



B.



C.



D.

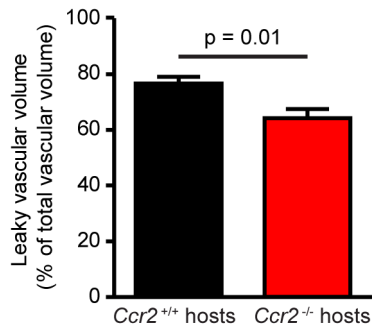


**Figure 9. Loss of stromal CCR2 expression improves doxorubicin response.** \*  $p < 0.05$  (Student's t-test). Error is depicted as mean  $\pm$  SEM.

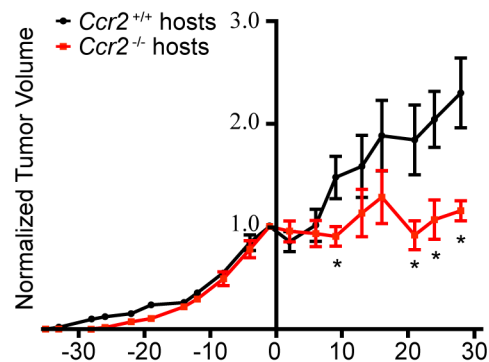
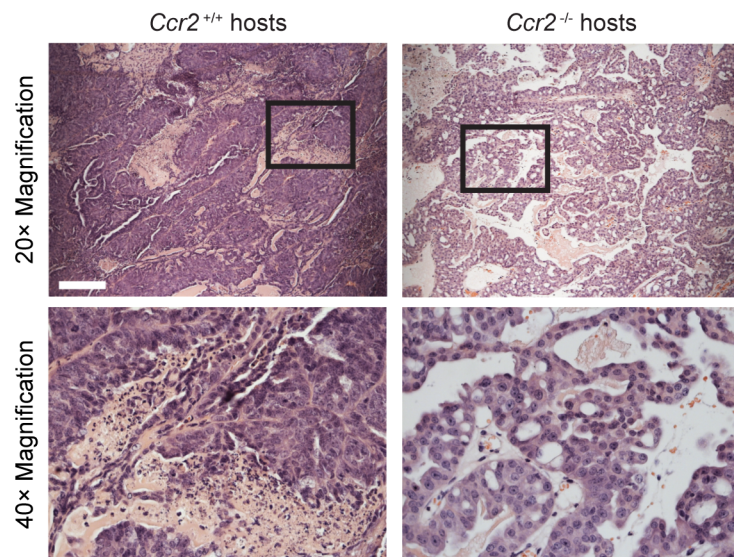


**Figure 10. Loss of CCR2 expression in the stromal compartment alters tumor histopathology.** Tumors of Ccr2<sup>-/-</sup> hosts are of a lower histological grade 6 weeks after the first dose of doxorubicin is administered.  $p = 0.005$ , Fisher's exact test. Scale = 100  $\mu$ m.



## II. Manuscript

The following proof of the accepted manuscript has been embargoed and cannot be released for public viewing until after the date of publication, as per the editor's request. The publication date for this manuscript is April 17, 2012.

# Imaging Tumor-Stroma Interactions during Chemotherapy Reveals Contributions of the Micro-Environment to Resistance

Elizabeth S. Nakasone,<sup>1,2,10</sup> Hanne A. Askautrud,<sup>1,3,4,5,10</sup> Tim Kees,<sup>1</sup> Jae-Hyun Park,<sup>1</sup> Vicki Plaks,<sup>3</sup> Andrew J. Ewald,<sup>3,6</sup> Miriam Fein,<sup>1,7</sup> Morten G. Rasch,<sup>1,8</sup> Ying-Xim Tan,<sup>3</sup> Jing Qiu,<sup>1</sup> Juwon Park,<sup>1</sup> Pranay Sinha,<sup>1</sup> Mina J. Bissell,<sup>9</sup> Eirik Frengen,<sup>4,5</sup> Zena Werb,<sup>3,11</sup> and Mikala Egeblad<sup>1,3,11,\*</sup>

<sup>1</sup>Cold Spring Harbor Laboratory

<sup>2</sup>Watson School of Biological Sciences  
Cold Spring Harbor, NY 11724, USA

<sup>3</sup>Department of Anatomy, University of California, San Francisco, San Francisco, CA 94143, USA

<sup>4</sup>Department of Medical Genetics, Institute of Clinical Medicine, University of Oslo, N-0315 Oslo, Norway

<sup>5</sup>Department of Medical Genetics, Oslo University Hospital, N-0424 Oslo, Norway

<sup>6</sup>Departments of Cell Biology and Oncology, Center for Cell Dynamics, Johns Hopkins School of Medicine, Baltimore, MD, 21205, USA

<sup>7</sup>Graduate Program in Genetics, Stony Brook University, Stony Brook, New York 11794, USA

<sup>8</sup>Finsen Laboratory, Copenhagen University Hospital, DK-1165 Copenhagen, Denmark

<sup>9</sup>Life Sciences Division, Lawrence Berkeley National Laboratory, Berkeley, CA 94720, USA

<sup>10</sup>These authors contributed equally to this work

<sup>11</sup>These authors contributed equally to this work

\*Correspondence: [egeblad@cshl.edu](mailto:egeblad@cshl.edu)

DOI 10.1016/j.ccr.2012.02.017

## SUMMARY

Little is known about the dynamics of cancer cell death in response to therapy in the tumor micro-environment. Intravital microscopy of chemotherapy-treated mouse mammary carcinomas allowed us to follow drug distribution, cell death, and tumor-stroma interactions. We observed associations between vascular leakage and response to doxorubicin, including improved response in matrix metalloproteinase-9 null mice that had increased vascular leakage. Furthermore, we observed CCR2-dependent infiltration of myeloid cells after treatment and that *Ccr2* null host mice responded better to treatment with doxorubicin or cisplatin. These data show that the micro-environment contributes critically to drug response via regulation of vascular permeability and innate immune cell infiltration. Thus, live imaging can be used to gain insights into drug responses in situ.

## INTRODUCTION

One of the major challenges in treating cancer is resistance to therapy. It is well appreciated that cancer cell intrinsic factors, such as genetic or epigenetic changes, can cause development of therapy resistance (Dean et al., 2005). Extrinsic factors in the micro-environment of certain organs, such as the bone marrow and thymus, can also confer resistance (Gilbert and Hemann, 2010; Meads et al., 2009). In these cases, resistance is mediated by factors secreted from stromal cells, such as IL-6. In addition,

impaired drug penetration through the extracellular matrix (ECM) influences drug response in primary solid tumors (Loeffler et al., 2006; Olive et al., 2009).

Surprisingly little is known about how cells in intact tumors respond to classical chemotherapies (Minchinton and Tannock, 2006; Rottenberg et al., 2010). Most of the knowledge about these responses has been obtained from cell culture or xenograft experiments, where cancer cells grow under conditions very different from the micro-environments of human tumors. Indeed, such experiments are often not predictive of drug

## Significance

It is well appreciated that intrinsic factors regulate chemoresponsiveness. Using in vivo microscopy of tumors, we show that extrinsic factors within the micro-environment support the development of chemoresistance by regulating drug distribution and the inflammatory response. These results have clinical implications, as myeloid cell infiltration is increased in human breast tumors after chemotherapy and the cellular composition of the immune infiltrate is a strong predictor of overall survival. Our data suggest that the response to classical chemotherapeutic drugs can be improved by changing the tumor micro-environment with agents that modify matrix metalloproteinase activity and chemokine signaling. Our study shows that observing the tumor response in real-time at cellular resolution can yield insights into the biology of chemoresistance.

responses in patients (Johnson et al., 2001; Minchinton and Tanock, 2006).

To investigate the role of the micro-environment in chemoresponsiveness, we chose a well-documented mouse model, the mammary tumor virus (MMTV) promoter-driven polyoma middle T oncogene (PyMT) model, that displays progressive stages of tumorigenesis similar to human luminal type B breast cancer (Herschkowitz et al., 2007; Lin et al., 2003). As MMTV-PyMT tumors progress, cancer cells undergo molecular changes, including increased expression of ErbB receptor family members (Lin et al., 2003). In parallel, the stromal micro-environment undergoes changes in blood vessel architecture, ECM composition, and immune cell infiltration (Egeblad et al., 2008, 2010).

## RESULTS

### Doxorubicin Induces Necrotic Cell Death In Vivo

Doxorubicin (Adriamycin) is a cytotoxic drug used to treat advanced breast cancer (Rouzier et al., 2005). To investigate the acute, cellular response to doxorubicin treatment in the context of the tumor micro-environment, we monitored mammary carcinomas in live mice using spinning disk confocal microscopy (Egeblad et al., 2008). MMTV-PyMT mice were crossbred with the ACTB-ECFP and c-fms-EGFP reporter mice to enable visualization of different tumor stages and tracking of the most abundant stromal cell type, myeloid cells (Egeblad et al., 2008). Dead cells were labeled with propidium iodide (PI) administered intraperitoneally (i.p.). Cell death became apparent 24–30 hr after doxorubicin administration and increased as imaging continued, whereas there was limited cell death in untreated control mice (Figure 1A; Figure S1A available online; see Figure 2 for quantification). The death of individual cells was readily observed as the appearance of PI staining (Figure 1B; Movie S1). In addition to cell death in the tumor mass, we observed stromal cell death (Figure 1A).

Necrosis is a major pathway of cell death after doxorubicin treatment in vitro (Obeid et al., 2007). Cell death by apoptosis and necrosis are characterized by specific changes in nuclear morphology and plasma membrane integrity (Dive et al., 1992). We next determined the nature of doxorubicin-induced cell death in vivo by imaging changes in nuclear morphology in MMTV-PyMT;ACTB-ECFP mice crossbred with mice expressing histone H2B conjugated to EGFP (Hadjantonakis and Papaioannou, 2004). The majority of the nuclei became positive for PI before their morphology changed, indicating early loss of plasma membrane integrity and necrosis-like cell death. A small percentage of cells died with breakdown of chromatin into condensed bodies followed by acquisition of PI labeling, indicating late loss of plasma membrane integrity and apoptosis-like cell death (Figures 1C and 1D; Movie S2). By histology, we observed only a minor increase in the number of cells with the condensed chromatin that is typical of apoptosis after doxorubicin treatment (Figure S1B). Thus, doxorubicin predominantly induces necrosis in vivo.

### Doxorubicin Sensitivity Changes with Tumor Stage

At the macroscopic level, doxorubicin treatment reduced tumor volume in MMTV-PyMT mice bearing multiple tumors (Figures

2A and S2A). However, the smallest or largest tumors tended to be resistant (Figure S2B), suggesting that resistance was associated with tumor progression.

MMTV-PyMT tumors have been classified into four pathological stages, based on cellular morphology, lack of basement membrane, and infiltration of immune cells (Lin et al., 2003). We adapted this classification to allow a simplified assessment of tumor stage in live animals: “hyperplasia,” small lesions showing increased accumulation of cells as compared to normal epithelium; “early carcinoma,” lesions with evidence of myeloid cell infiltration and/or cancer cell invasion; and “late carcinoma,” large lesions with densely packed cancer cells (Egeblad et al., 2008). MMTV-PyMT mammary glands have multiple tumors, which are often at different stages of progression. This allowed us to image doxorubicin response at different stages in the same mouse (Figures 2B and S2C). Cell death increased after doxorubicin-treatment in early carcinomas (Figure 2C); on average, 10% of the fields of view (FOV) were positive for PI at 31 hr after doxorubicin-treatment compared to 2% of the FOV in the controls (Figure S2D). In contrast, cell death did not increase in hyperplasias and late carcinomas after treatment (Figures 2B, 2C, S2C, and S2D; Movie S3), suggesting marked differences in drug sensitivity between tumor stages. Cancer cells in early carcinomas also accumulated more DNA damage after doxorubicin treatment than those in hyperplasias or late carcinomas, as determined by immunostaining for histone  $\gamma$ -H2AX (Figure 2D). Thus, doxorubicin sensitivity changes with tumor stage but not in a linear manner.

### Cancer Cell Proliferation Does Not Correspond to Doxorubicin Sensitivity In Vivo

Doxorubicin intercalates into DNA, inhibiting topoisomerase II. Hence, proliferating cells are predicted to be more sensitive than resting cells (Campiglio et al., 2003). Yet, cancer cell proliferation differed insignificantly between tumor stages (Figure 2E). Furthermore, in pulse-chase experiments, the percentage of dead cells that were BrdU<sup>+</sup> was similar in doxorubicin- and phosphate buffered saline (PBS)-treated tumors (Figure 2F). These data suggest that differences in cellular proliferation between tumor stages are not the main cause of differences in doxorubicin sensitivity in vivo.

### Primary Cancer Cells from Different Tumor Stages Do Not Exhibit Intrinsic Differences in Doxorubicin Sensitivity in Culture

As tumors progress, cancer cells acquire mutations and silence or activate genes. These changes can give rise to differences in sensitivity between tumor stages. To distinguish the contribution of cancer cell intrinsic changes from those of the tissue micro-environment, we isolated cancer cells from MMTV-PyMT; ACTB-ECFP mice using a fluorescent dissection microscope. This allowed us to visualize the cancer epithelium during tissue removal, ensuring that tumors were representative of the different stages (Figure S2E). Indeed, in vitro sensitivity to the ErbB1/ErbB2 inhibitor lapatinib was highest for cells isolated from late carcinomas (Figure 2G), as predicted from the increased expression of the ErbB2/Neu oncoprotein in late-stage tumors (Lin et al., 2003). In contrast, cells from hyperplasia, early carcinoma, and late carcinoma stages had similar

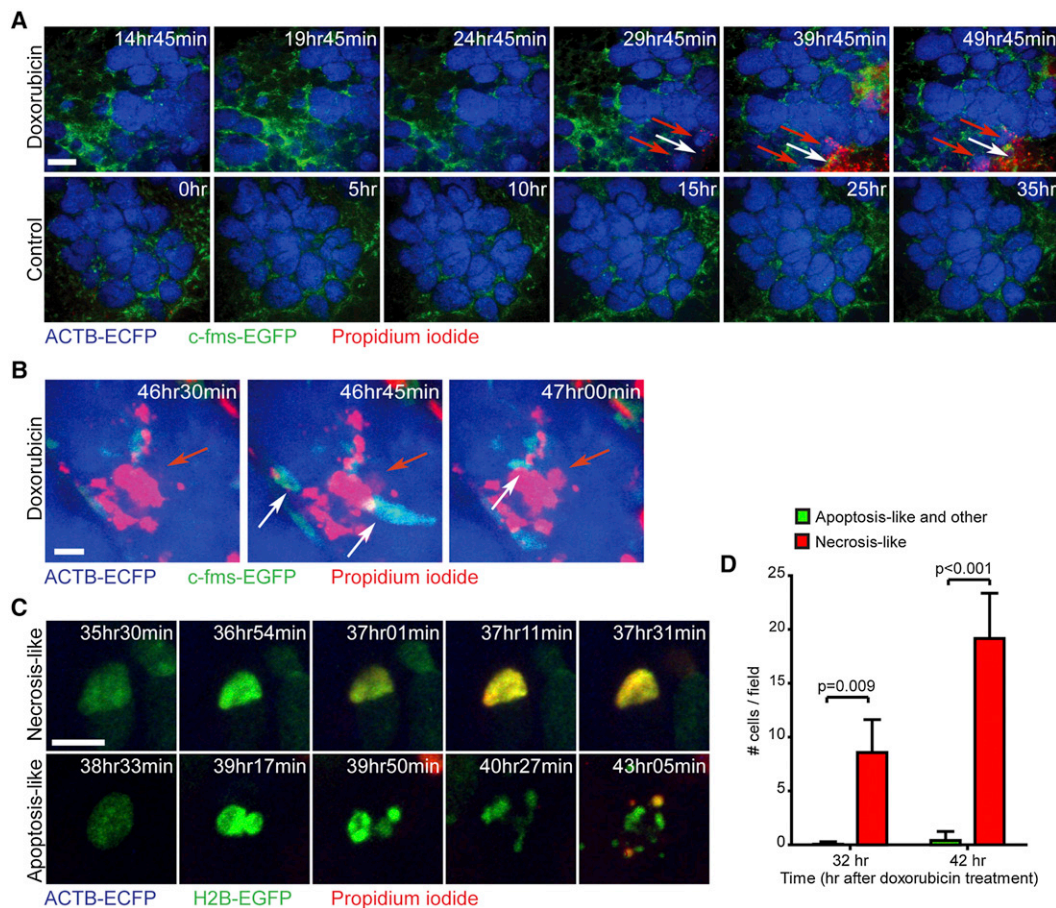


**Figure 1. Visualizing Cellular Responses to Chemotherapy In Vivo**

(A) Doxorubicin-induced cell death in tumors of live MMTV-PyMT;ACTB-ECFP;c-fms-EGFP mice. Induction of cell death (red), visualized by propidium iodide (PI) uptake, can be seen in a tumor lesion (blue) infiltrated with myeloid cells (green). Red arrows point to cell death in the tumor, and white arrows point to cell death in the stroma. Time after treatment (doxorubicin) or initiation of imaging (control) is indicated. Scale bar: 100  $\mu$ m.

(B) Dynamics of cell death in situ. Single cell death was observed as the appearance of PI staining (red arrow). This was followed by myeloid cell infiltration (white arrows). Time after doxorubicin treatment is indicated. Scale bar: 10  $\mu$ m.

(C) Dynamics and types of nuclear structural changes after doxorubicin treatment in MMTV-PyMT;ACTB-ECFP;H2B-EGFP mice. Examples of necrosis-like (nucleus becomes PI<sup>+</sup> without major structural changes) and apoptosis-like cell death (nuclear structure breakdown before PI uptake). Time after treatment is indicated. Scale bar: 10  $\mu$ m.

(D) Doxorubicin induces necrosis-like cell death (mean  $\pm$  SEM; 18 fields of view [FOV] from three mice were counted;  $p = 0.009$  at 32 hr,  $p < 0.001$  at 42 hr, Student's  $t$  test).

Also see [Figure S1](#) and [Movies S1](#) and [S2](#).

sensitivity to doxorubicin in both two- and three-dimensional cultures ([Figures 2H](#), [2I](#), and [S2F](#)). Primary macrophages and the macrophage cell line RAW 264.7 were also sensitive to doxorubicin ([Figure S2G](#)), in accordance with the stromal cell death observed by imaging. Taken together, the *in vitro* data indicated that cancer cell intrinsic mechanisms are unlikely to be responsible for the differences in doxorubicin sensitivity that were observed between tumor stages and that extrinsic mechanisms are operative *in vivo*.

### Visualization of Drug Distribution in Real-Time Reveals Its Association with Drug Response

Interstitial fluid pressure is one extrinsic factor that increases in late-stage tumors as compared to early stages and it hinders drug penetration into tumors ([Hagendoorn et al.](#),

[2006](#); [Netti et al.](#), 1999). Therefore, we hypothesized that differences in drug response between tumor stages might be related to differences in drug accessibility. Doxorubicin is naturally fluorescent, allowing for imaging of its distribution. However, its broad emission and excitation spectra overlap with those of our fluorescent reporters. It was therefore not possible to image doxorubicin distribution in MMTV-PyMT;ACTB-ECFP mice in which tumor stage could be determined. Instead, we imaged unlabeled MMTV-PyMT mice and identified tumor areas by palpation and abnormal tumor vasculature, visualized using intravenously (i.v.) injected fluorescent nanoparticles (AngioSPARK 680, PerkinElmer, Waltham, MA, USA).

We imaged small (just palpable), medium ( $\sim 160$  mm<sup>3</sup>), and large ( $\sim 845$  mm<sup>3</sup>) tumors ([Figure 3A](#); [Movies S4](#) and [S5](#)).

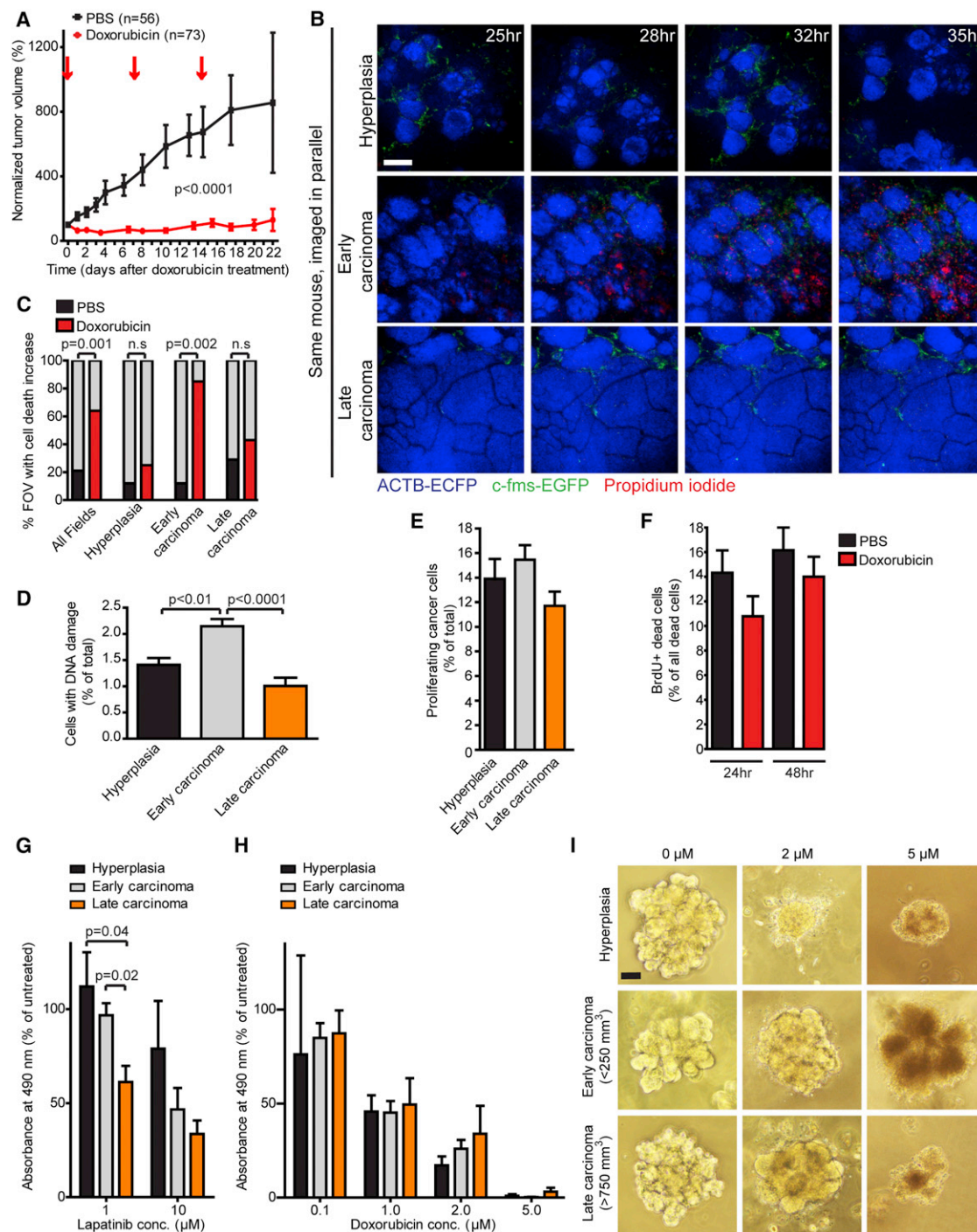


**Figure 2. Doxorubicin Sensitivity Changes with Tumor Stage In Vivo but Not In Vitro**

(A) Doxorubicin treatment reduces tumor volume in MMTV-PyMT mice. Mice were given doxorubicin or PBS at days 0, 7, and 14 (indicated by arrows). Analysis includes 73 tumors from eleven doxorubicin-treated mice and 56 tumors from 12 PBS-treated mice (mean  $\pm$  SEM,  $p < 0.0001$  for all time-points, Student's *t* test). (B) Doxorubicin-induced cell death preferentially occurs in early carcinomas and not in hyperplasias and late carcinomas. Different micro-environments imaged in the same MMTV-PyMT;ACTB-ECFP;c-fms-EGFP mouse after doxorubicin treatment. Time after treatment is indicated. Scale bar: 100  $\mu m$ . (C) Cell death increases between 24 and 36 hr after doxorubicin treatment ( $n = 25$  fields of view [FOV]) as compared to control mice imaged for similar time frames ( $n = 23$  FOV; Fisher's exact test;  $p = 0.001$ ). Cell death increases in early carcinomas (12 of 14 doxorubicin-treated versus 1 of 8 control-treated FOV, Fisher's exact test,  $p = 0.002$ ) but not in hyperplasias (1 of 4 versus 1 of 8 fields) or late carcinomas (3 of 7 versus 2 of 7). Four control- and four doxorubicin-treated mice were imaged. (D) DNA damage response measured by  $\gamma$ -H2AX immunostaining differs between tumor stages (mean  $\pm$  SEM, analysis of variance [ANOVA],  $p < 0.0001$ ) and is higher in early carcinomas ( $p < 0.01$ , Bonferroni posttest) or late carcinomas ( $p < 0.0001$ ; Bonferroni posttest; 21 hyperplasia, 25 early carcinoma, and 24 late carcinoma FOV were evaluated in five tumors from five mice).

Doxorubicin rapidly leaked out into the tissue and accumulated in the nuclei of cells near blood vessels (Figure 3A). This resulted in an intravascular half-life of 9.5 min (range, 7.9–11.8 min; Figure 3B), consistent with the initial plasma half-life of 8.5 min (range, 7.2–9.8 min) reported in human patients (Greene et al., 1983). Doxorubicin distribution varied among tumors of different sizes (Figures 3A and 3C), with the most leakage in larger tumors and the least leakage in those that were just palpable. Furthermore, significantly more doxorubicin was extractable from small tumors (13–81 mm<sup>3</sup>) than from hyperplastic MMTV-PyMT tissues or normal mammary glands (Figure 3D). Solid tumors tend to have progressed further than softer ones, and when tumors were analyzed based on consistency, as well as size, the highest levels of doxorubicin were found in soft tumors, although the values were not significantly higher than in solid tumors of similar size (Figure 3E).

Tumor size and consistency is not an accurate indicator of tumor stage. Thus, to quantify vascular leakage in tumors of different stages, we co-injected i.v. fluorescent 10 kD (low) and 2 MD (high) molecular mass dextrans into MMTV-PyMT;ACTB-ECFP mice (Figures 4A and S3A; Movie S6). The intravascular half-lives of dextrans were similar in tumor micro-environments at different stages (Figures S3B and S3C), with a higher intravascular half-life for 2 MD dextran (41 [range, 32–58] min) than for 10 kD dextran (15 [range, 14–16] min; Figure S3D).

In contrast to intravascular half-life, leakage of dextrans into the extravascular space and their retention in tissues were clearly influenced by tumor stage (Figures 4A and 4B). Regions with hyperplasias showed limited leakage into the extravascular space, whereas early carcinomas and the tumor-stroma borders of late carcinomas exhibited substantially more leakage. Extravasated 10 kD dextran reached a larger area of the tissue than did extravasated 2 MD dextran (Figures 4A and 4B). Following extravasation, the dextrans accumulated in stromal cells, which we have previously shown are c-fms<sup>+</sup>CD68<sup>+</sup>CD206<sup>+</sup> macrophages (Egeblad et al., 2008). Leakage in normal mammary glands was minimal and below detection limits when the settings used for tumor-bearing mice were applied (not shown).

Finally, we co-injected i.v. doxorubicin-treated mice with 10 kD dextran and *Ricinus communis* agglutinin I, a lectin that binds to basement membrane exposed to the vascular lumen, marking leaky vasculature (Thurston et al., 1999). We observed that only tumor areas in close proximity to these two markers contained cells with nuclear uptake of doxorubicin (Figure S3E). Interestingly, some of the cells with doxorubicin-positive nuclei had also taken up dextran, suggesting that they were macrophages (Figure S3E).

### Absence of MMP9 Results in Increased Vascular Leakage and Sensitizes Tumors to Doxorubicin Treatment

Tumor-associated macrophages promote vascular changes (Egeblad et al., 2010). We found that the extent of local c-fms-EGFP<sup>+</sup> myeloid cell infiltration correlated significantly with the degree of local 10 kD dextran leakage, regardless of tumor stage (Figures 4C and 4D). Myeloid cells can regulate vessel stability via secretion of vascular endothelial growth factor (VEGF) and transforming growth factor (TGF)- $\beta$ , both of which are sequestered in the ECM and released by matrix metalloproteinases (MMPs; Yu and Stamenkovic, 2000; Ebrahim et al., 2010). Nevertheless, MMPs may also negatively regulate vascular permeability (Sounni et al., 2010). Several MMPs, including MMP9, are expressed at high levels by tumor-infiltrating myeloid cells (Figure 5A). To determine if host-derived MMP9 affects vascular stability and doxorubicin response, we transplanted MMTV-PyMT cancer cells to wild-type FVB/n and *Mmp9*<sup>-/-</sup> hosts and treated them with doxorubicin. Although MMP9 does not influence primary tumor growth in the transgenic MMTV-PyMT model (Martin et al., 2008), we found that the growth of grafted tumors was reduced in *Mmp9*<sup>-/-</sup> hosts compared to FVB/n hosts (Figure S4A). Interestingly, tumors in *Mmp9*<sup>-/-</sup> hosts responded better to doxorubicin than those in FVB/n hosts (Figure S4B).

Since transplanted MMTV-PyMT tumors grew slower in *Mmp9*<sup>-/-</sup> hosts, we could not rule out that the influence of MMP9 on doxorubicin response was related to its effects on cancer cell proliferation. Therefore, we tested if MMP9 influenced the response in the MMTV-Neu model, another doxorubicin-sensitive, luminal breast cancer model, in which the absence of MMP9 does not affect cancer cell proliferation or tumor growth (Figures S4C and S4D; data not shown). Vascular volume, determined by i.v. tomato lectin staining, was not affected by MMP9 status, but tumor vessels were leakier in the absence of MMP9, as determined by i.v. staining with *Ricinus communis* agglutinin I (Figures 5B–5D). In the absence of MMP9, the endothelial cell adhesion molecule VE-cadherin showed increased phosphorylation (Figures 5E and 5F), which results in loose adherence junctions (Gavard, 2009). Vascular coverage with pericytes, which support endothelial cells, was also decreased (Figures 5G and S4E). In keeping with the increased permeability of the vasculature, MMTV-Neu;*Mmp9*<sup>-/-</sup> tumors treated with doxorubicin responded better than did MMTV-Neu;*Mmp9*<sup>+/+</sup> tumors (Figure 5H). In contrast, C3(1)-Tag tumors, a basal-like mammary carcinoma model that is largely doxorubicin-resistant (Figure S4F), did not respond better in the absence of MMP9 (Figure S4G).

(E) Cancer cell proliferation determined by BrdU labeling does not differ between tumor stages in MMTV-PyMT mice (mean  $\pm$  SEM, not significant, n.s., ANOVA; 13 hyperplasia, 19 early carcinoma, and 28 late carcinoma FOV were evaluated in six tumors from three mice).

(F) Proliferating (BrdU<sup>+</sup>) cells are not preferentially killed by doxorubicin treatment. The fraction of BrdU<sup>+</sup> cells with cell-death-associated nuclear changes was scored (mean  $\pm$  SEM, n.s., Student's t test; for each condition, 58–60 FOV were analyzed in six tumors from three mice).

(G) Sensitivity to the ErbB1/ErbB2 inhibitor lapatinib is highest for cancer cells from late-stage tumors in culture (mean  $\pm$  SEM,  $p = 0.04$  or  $0.02$  as indicated, Student's t test; values represent the averages of four experiments, each done in triplicate with primary cells from independent mice).

(H) Sensitivity to doxorubicin is not affected by tumor stage in culture (mean  $\pm$  SEM, n.s., ANOVA; values represent the averages of four experiments, each done in triplicate with primary cells from independent mice).

(I) Morphology of organoids generated from tumors at different stages after treatment with the indicated concentrations of doxorubicin. Scale bar: 50  $\mu$ m. Also see Figure S2 and Movie S3.

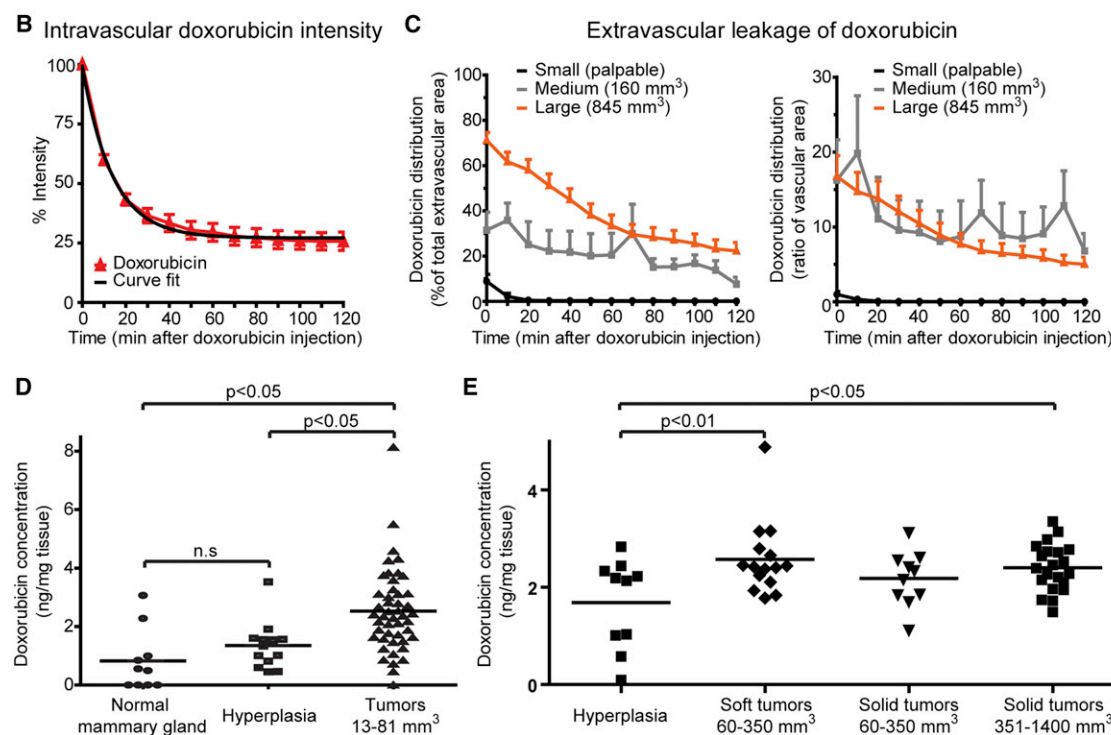
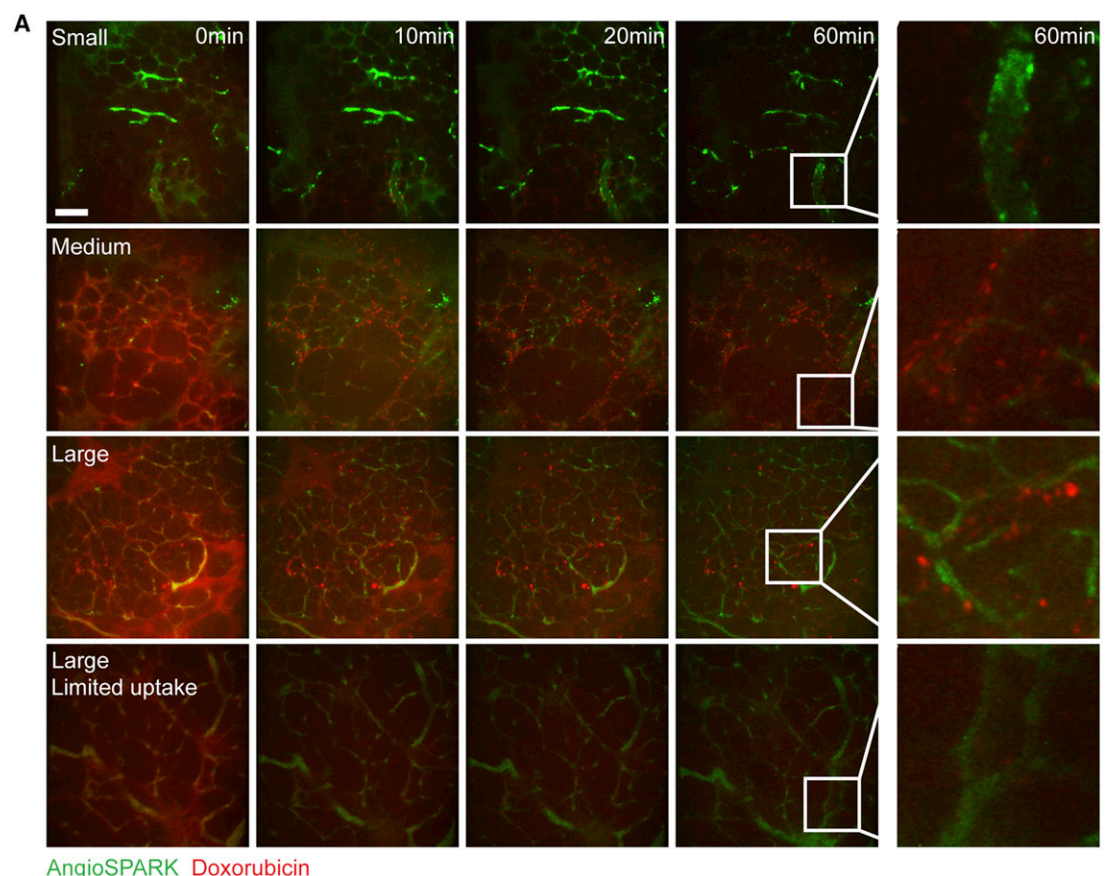


**Figure 3. Distribution and Uptake of Doxorubicin in Different Tumor Sizes**

(A) Doxorubicin leakage and uptake varies with tumor size. MMTV-PyMT mice with small (just palpable tumors), medium (~160 mm<sup>3</sup>), or large tumors (~845 mm<sup>3</sup>) were injected intravenously with AngioSPARK 680 (green) and doxorubicin (red). Minimal leakage and uptake were seen in small tumors. Leakage was high in

### Doxorubicin Treatment Leads to Recruitment of Myeloid Cells to Tumors

We observed that vascular leakage was associated with higher infiltration of macrophages (Figure 4D), so we sought to determine the effect of MMP9 on macrophage infiltration. There were increased numbers of cells expressing the F4/80 and CD206 macrophage markers in untreated tumors of *Mmp9*<sup>-/-</sup> hosts compared to those of FVB/n hosts (Figures 6A and 6B). Interestingly, doxorubicin treatment significantly reduced the number of macrophages in *Mmp9*<sup>-/-</sup> hosts, suggesting that macrophages were killed.

Despite the reduction in macrophage numbers observed after doxorubicin-treatment of *Mmp9*<sup>-/-</sup> hosts, imaging consistently showed recruitment of myeloid cells to doxorubicin-treated tumors in wild-type mice (Figures 6C and 6D; Movie S7). These myeloid cells often formed granuloma-like structures in areas with cell death (Movie S7). Rarely, we observed myeloid cell recruitment prior to cancer cell death (Figure S5A).

Myeloid cells are a diverse family of innate immune cells, including neutrophils, monocytes, and macrophages, that are all recruited to areas of cell death (Murdoch et al., 2004). To determine a basis for myeloid cell infiltration, we injected necrotic cell debris into mammary glands of non-tumor-bearing mice and imaged the response. In this model, the results are independent of any direct effects of doxorubicin on myeloid cells, such as induction of cell death. Myeloid cell infiltration increased in areas injected with necrotic debris as compared to areas injected with only saline and dextran (Figure S5B). Once a myeloid cell recognized the cell debris, other myeloid cells were rapidly recruited and a granuloma-like structure was formed (Figure S5B; Movie S8). Myeloid cell recruitment is often mediated by G<sub>i</sub>-protein coupled chemokine receptors (Sadik et al., 2011). Mice pretreated with pertussis toxin, a G<sub>i</sub>-protein inhibitor, showed reduced myeloid cell recruitment to cell debris, suggesting the involvement of chemokine receptors in this process (Figure S5C; Movie S9).

### Myeloid Cells Are Recruited to Doxorubicin-Treated Tumors through a Stromal CCL2/CCR2 Chemokine/Chemokine Receptor Axis

To screen for candidate chemokines involved in the recruitment of myeloid cells, we used a protein array. Tumor lysates isolated 48 hr after doxorubicin treatment showed increased protein levels for CCL2 and CCL12 (Figure 7A). Both of these

chemokines are ligands for the CCR2 receptor, which is expressed on monocytes and is responsible for their recruitment to sites of inflammation (Tsou et al., 2007). We also observed small increases in macrophage colony-stimulating factor (M-CSF/CSF1) and tissue inhibitor of metalloproteinase 1 (TIMP1; Figure 7A). We confirmed the increases in CCL2 and CCL12 by enzyme-linked immunosorbent assay and immunostaining (Figures 7B, S6A, and S6B). CCL2-expressing cells were large cells located in the stroma that did not express markers of fibroblasts and pericytes (Figure 7C) or endothelial cells (Figure 7D).

Next, we investigated the types of myeloid cells recruited after doxorubicin treatment. Infiltration of cells expressing a neutrophil/monocyte marker, the 7/4 antigen (Ly6B.2), was significantly increased (Figure 7E). This increase was exclusively found among cells that also expressed the CCL2 receptor, CCR2, and had a monocytic nuclear morphology (Figures 7E and S6C). The number of 7/4<sup>+</sup>CCR2<sup>-</sup> cells did not increase but rather decreased, after doxorubicin treatment (Figure 7E). A small number of CCR2<sup>+</sup> cells did not express the 7/4 antigen, but their numbers did not change after doxorubicin treatment (Figure 7E). In contrast to the acute increase in the infiltration of 7/4<sup>+</sup>CCR2<sup>+</sup> cells, overall macrophage infiltration, as determined by the F4/80 marker, was not changed 48 hr after doxorubicin treatment (Figure S6D). However, a small increase was seen in the number of cells within the tumor mass that expressed CD206, a marker of alternatively activated macrophages (Figure S6E).

We next tested whether CCR2 mediates the myeloid cell infiltration seen after doxorubicin treatment. We transplanted primary cancer cells isolated from MMTV-PyMT mice to *Ccr2*<sup>-/-</sup> or C57BL/6 hosts and characterized the myeloid cell population after doxorubicin treatment. In C57BL/6 hosts, the fraction of cells co-expressing the myeloid cell marker CD11b with the monocyte/neutrophil markers Gr1 and 7/4 increased significantly after doxorubicin treatment (Figures 7F and 7G). The total proportion of cells in the tumors that expressed the myeloid CD11b marker did not increase (Figure S6F). Tumors of *Ccr2*<sup>-/-</sup> hosts had a higher fraction of CD11b<sup>+</sup>7/4<sup>+</sup>Gr1<sup>+</sup> cells than did C57BL/6 hosts (Figures 7F and 7G), consistent with previous reports (Pahler et al., 2008). However, there was no significant increase in this cell population after doxorubicin treatment in *Ccr2*<sup>-/-</sup> hosts (Figures 7F and 7G). Doxorubicin treatment did not affect the subpopulations of CD11b<sup>+</sup> cells that expressed

medium and some large tumors, with variable nuclear retention. Time after doxorubicin injection is indicated. The last column shows nuclear uptake of doxorubicin (higher magnification of the areas outlined in the fourth column). Scale bar: 100  $\mu$ m.

(B) Decay of intravascular doxorubicin levels determined by imaging is modeled as one-phase exponential decay (black line; mean  $\pm$  SEM; eight FOV from two mice were analyzed).

(C) Kinetics of doxorubicin leakage from vessels in tumors of different sizes. Quantification of the percentage of extravascular pixels with doxorubicin signal above intensity threshold (150% of background) and as a ratio of extravascular doxorubicin to vascular area (mean  $\pm$  SEM; eight small, four medium, and eleven large FOV were analyzed in six mice).

(D) Doxorubicin concentration is higher in tumors than hyperplasias and normal mammary glands (means are shown;  $p < 0.0001$ , ANOVA, and Bonferroni posttests for comparison of groups;  $p < 0.05$  or n.s. as indicated; ten normal mammary glands from five FVB/n mice and 14 hyperplastic and 47 tumors [13–81 mm<sup>3</sup>] from five MMTV-PyMT were analyzed).

(E) Doxorubicin concentration is higher in tumors that were soft upon dissection than in hyperplastic tissue or solid tumors of similar size (means are shown,  $p = 0.01$ , ANOVA, and Bonferroni posttests for comparison of groups,  $p < 0.01$  or 0.05 as indicated). Ten hyperplastic, 15 soft and medium-sized (60–350 mm<sup>3</sup>), ten solid and medium-sized (60–350 mm<sup>3</sup>), and 21 solid and large tumors (351–1,400 mm<sup>3</sup>) from five MMTV-PyMT mice were analyzed.

Also see Movies S4 and S5.

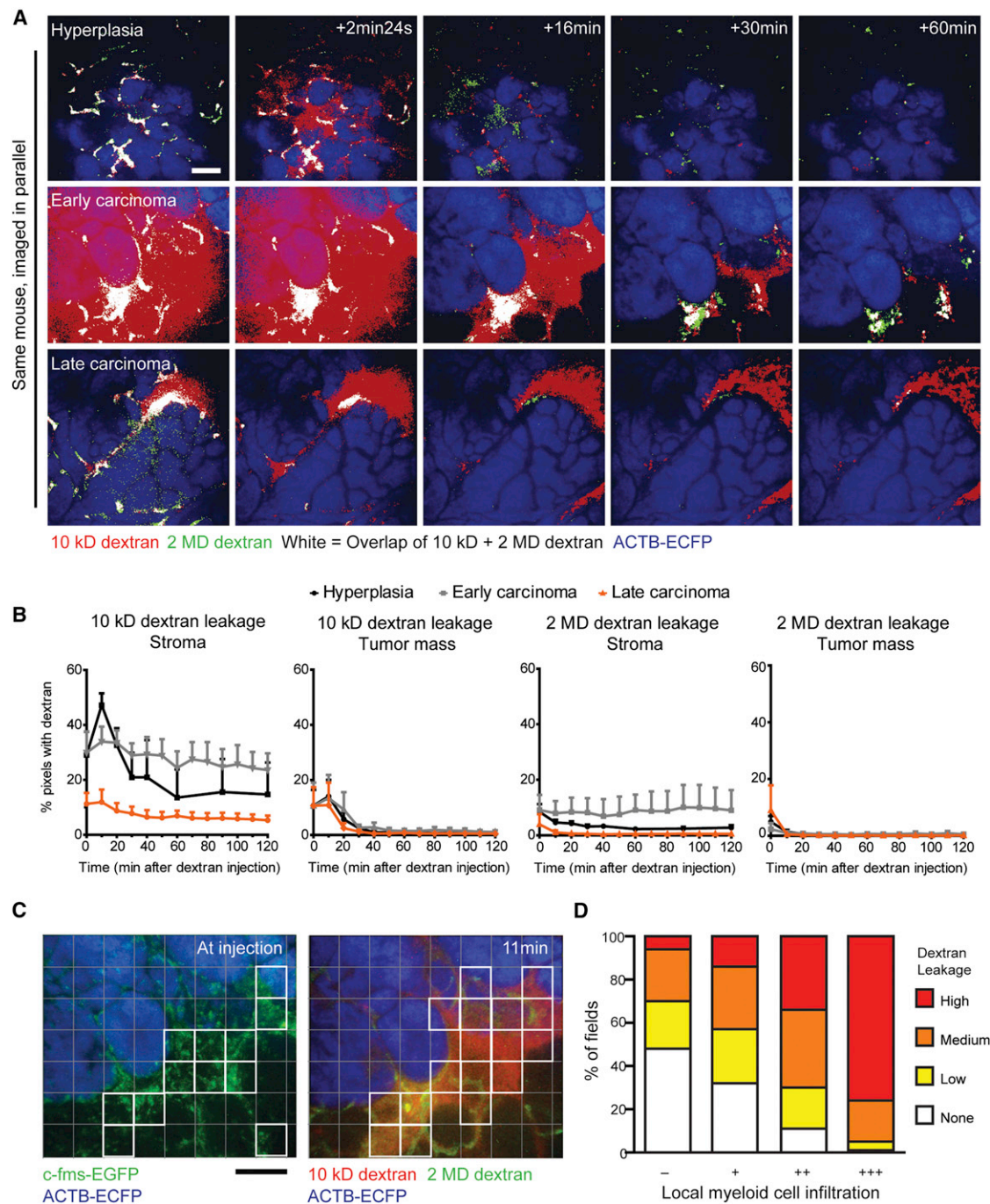


**Figure 4. Leakage and Distribution of Intravenously Injected Dextran Varies with Tumor Stage**

(A) Early carcinomas exhibit a higher degree of dextran leakage than do hyperplasias and late carcinomas. More extensive leakage of 10 kD than 2 MD dextran is shown for all tumor stages. Kinetics of 10 kD (red) and 2 MD dextran (green) leakage from vessels in three different tumor stages from the same MMTV-PyMT; ACTB-ECFP mouse are shown. Regions with leakage of both dextrans are depicted in white and the epithelium in blue (ACTB-ECFP). Time after dextran injection is indicated. Scale bar: 100  $\mu$ m.

(B) Quantification of the percentage of pixels above intensity threshold (150% of background) for the two dextrans in the epithelial and stromal compartments (mean  $\pm$  SEM; four hyperplasias from two mice, five early carcinomas from four mice, and five late carcinomas from four mice were analyzed).

(C) The extent of c-fms-EGFP<sup>+</sup> myeloid cell infiltration in MMTV-PyMT;ACTB-ECFP;c-fms-EGFP mice and the degree of 10 kD dextran leakage were scored independently using the indicated pixel grid. Co-injected 2 MD dextran was used to differentiate between intra- and extravascular 10 kD dextran. Examples of pixel fields scored as maximal infiltration and leakage are indicated by the white boxes. Scale bar: 100  $\mu$ m.

(D) Myeloid cell infiltration correlates with dextran leakage ( $r = 0.56$  and  $r = 0.47$ , for observer A and B, respectively,  $p < 0.0001$ , Spearman's rank correlation coefficient; 720 FOV from two mice were scored).

Also see Figure S3 and Movie S6.

F4/80 or CXCR4 in either genotype (Figures S6G–S6I). Together, our results suggest that doxorubicin treatment leads to a specific, acute recruitment of CCR2-expressing myeloid cells of the monocytic lineage through stromally expressed CCL2.

### Host CCR2 Influences Tumor Response to Chemotherapy

To determine if CCR2-mediated recruitment of myeloid cells influenced the response to doxorubicin, we generated cohorts of MMTV-PyMT;*Ccr2*<sup>+/-</sup> and MMTV-PyMT;*Ccr2*<sup>-/-</sup> mice. For doxorubicin-sensitive tumors (250–750 mm<sup>3</sup>), the absence of CCR2 was associated with a significantly better response, although tumors in both cohorts ultimately relapsed (Figure 8A). In contrast, tumors below 250 mm<sup>3</sup>, which respond poorly to doxorubicin, did not show a better response to treatment when mice were deficient for CCR2 (Figure S7A).

CCL2 has been proposed to promote cancer cell survival through CCR2 receptors on cancer cells (Zhang et al., 2010). To rule out the involvement of CCR2 signaling in cancer cells, we transplanted primary cancer cells from MMTV-PyMT mice to *Ccr2*<sup>-/-</sup> or C57BL/6 hosts. When treated with doxorubicin or cisplatin, a different class of chemotherapeutic drug with efficacy against MMTV-PyMT tumors (Figure S7B), tumors in *Ccr2*<sup>-/-</sup> hosts relapsed later than those in C57BL/6 hosts (Figures 8B and 8C). Tumor growth before treatment was not significantly different between *Ccr2*<sup>-/-</sup> and C57BL/6 hosts (Figure 8B). Myeloid cells can secrete factors that increase cancer cell survival (Shree et al., 2011). However, we detected no lasting survival benefit on primary cancer cells when they were cultured with primary macrophages (Figures S7C and S7D).

Although tumors in *Ccr2*<sup>-/-</sup> hosts relapsed, they were of a strikingly lower histological grade than the high-grade relapsed tumors of C57BL/6 hosts (Figure 8D). Histological differences were already evident 48 hr after doxorubicin treatment as tumors in *Ccr2*<sup>-/-</sup> hosts were more cystic than those in C57BL/6 hosts (Figure 8D). Taken together, our data suggest that infiltration of CCR2-expressing myeloid cells into chemotherapy-treated tumors contributes to tumor regrowth after treatment.

Like CCR2, MMP9 can also influence myeloid cell recruitment (Gong et al., 2008). We therefore tested whether the effects of MMP9 on doxorubicin response could be explained by effects on the acute recruitment of myeloid cells to treated tumors. However, adaptively transferred bone marrow cells from c-fms-EGFP;*Mmp9*<sup>+/-</sup> and c-fms-EGFP;*Mmp9*<sup>-/-</sup> mice were recruited equally well to tumors of MMTV-PyMT mice after treatment with doxorubicin (Figure S7E). Next, we tested whether the changed myeloid cell environment in *Ccr2*<sup>-/-</sup> mice correlated with vascular changes, akin to the effects of loss of *Mmp9* (Figure 8E). Whereas the vascular volume was higher in tumors of *Ccr2*<sup>-/-</sup> mice (Figure 8F), the percentage that was leaky was significantly lower, with the net result being no change in the total volume of leaky vasculature (Figures 8G and 8H). Furthermore, pericyte coverage of the vasculature was increased in *Ccr2*<sup>-/-</sup> hosts, whereas VE-cadherin phosphorylation levels were unaffected (Figures S7F–S7I). Thus, although the response to doxorubicin is improved in both *Mmp9*<sup>-/-</sup> and *Ccr2*<sup>-/-</sup> microenvironments, the effects on vascular structure and myeloid cell recruitment after treatment are different.

### DISCUSSION

We imaged the dynamics of doxorubicin responses in a progressive cancer model and revealed that chemosensitivity in vivo is influenced by the tumor microenvironment. The highest sensitivity to doxorubicin was not observed in the earliest or latest tumor stages but rather in the intermediate stage. These differences in drug response between stages were associated with parallel differences in vascular leakage. We therefore tested doxorubicin response in *Mmp9* null tumor microenvironments with increased vascular permeability and found an improved response. Doxorubicin treatment led to the recruitment of CCR2<sup>+</sup> monocytic cells to tumors. In *Ccr2* null micro-environments, recruitment was inhibited and the response to chemotherapy better. These results have clinical implications, as myeloid cell infiltration is increased in human breast tumors after chemotherapy and the composition of the immune infiltrate is a predictor of survival (Denardo et al., 2011).

### Stromal Regulation of Vascular Leakage

Primary cancer cells from different stages responded similarly to doxorubicin in vitro, whereas doxorubicin sensitivity, tumor stage, and vascular leakage were related in vivo. This suggests that stage-specific changes in vascular leakage contributed to doxorubicin response although we cannot exclude contributions from stromal cells. Strikingly, increased leakage of the tumor vasculature in *Mmp9*<sup>-/-</sup> mice corresponded to a better response to doxorubicin. The increased vascular permeability in *Mmp9*<sup>-/-</sup> mice was associated with decreased pericyte-coverage of the vasculature and increased phosphorylation of VE-cadherin, which affect endothelial cell-cell adhesions (Gavard, 2009; Goel et al., 2011). Although MMP inhibitors have failed in clinical trials (Coussens et al., 2002), our data suggest that these, or other drugs that affect vascular permeability, could be used to achieve better responses to chemotherapies.

MMP9 may regulate vascular structure by acting on a substrate in the tumor micro-environment. Indeed, a reduction of infiltrating MMP9<sup>+</sup> myeloid cells through inhibition of the CSF-1 receptor results in a better response to anti-VEGFR2 treatment (Priceman et al., 2010). However, MMP9 may also regulate vascular permeability indirectly through its effects on macrophage infiltration. Macrophages can secrete VEGF (also known as vascular permeability factor), which induces VE-cadherin phosphorylation in endothelial cells (Gavard, 2009).

Myeloid cells are not the only stromal cells capable of regulating drug delivery in tumors. By decreasing the fibroblast pool, and thus the ECM, drugs better enter the tissue (Loeffler et al., 2006; Olive et al., 2009). Interestingly, the improved drug delivery in these cases is achieved by increased vascular density and “vascular normalization,” which involves better pericyte coverage and reduced permeability (Goel et al., 2011). Since vascular volume and pericyte coverage increased in tumors of *Ccr2*<sup>-/-</sup> compared to C57BL/6 hosts, such vascular changes could play a role in the MMTV-PyMT model. Untangling the roles of MMP9 and CCR2 on vasculature, myeloid cell infiltration, and drug response will require the ability to temporally and conditionally manipulate these genes.

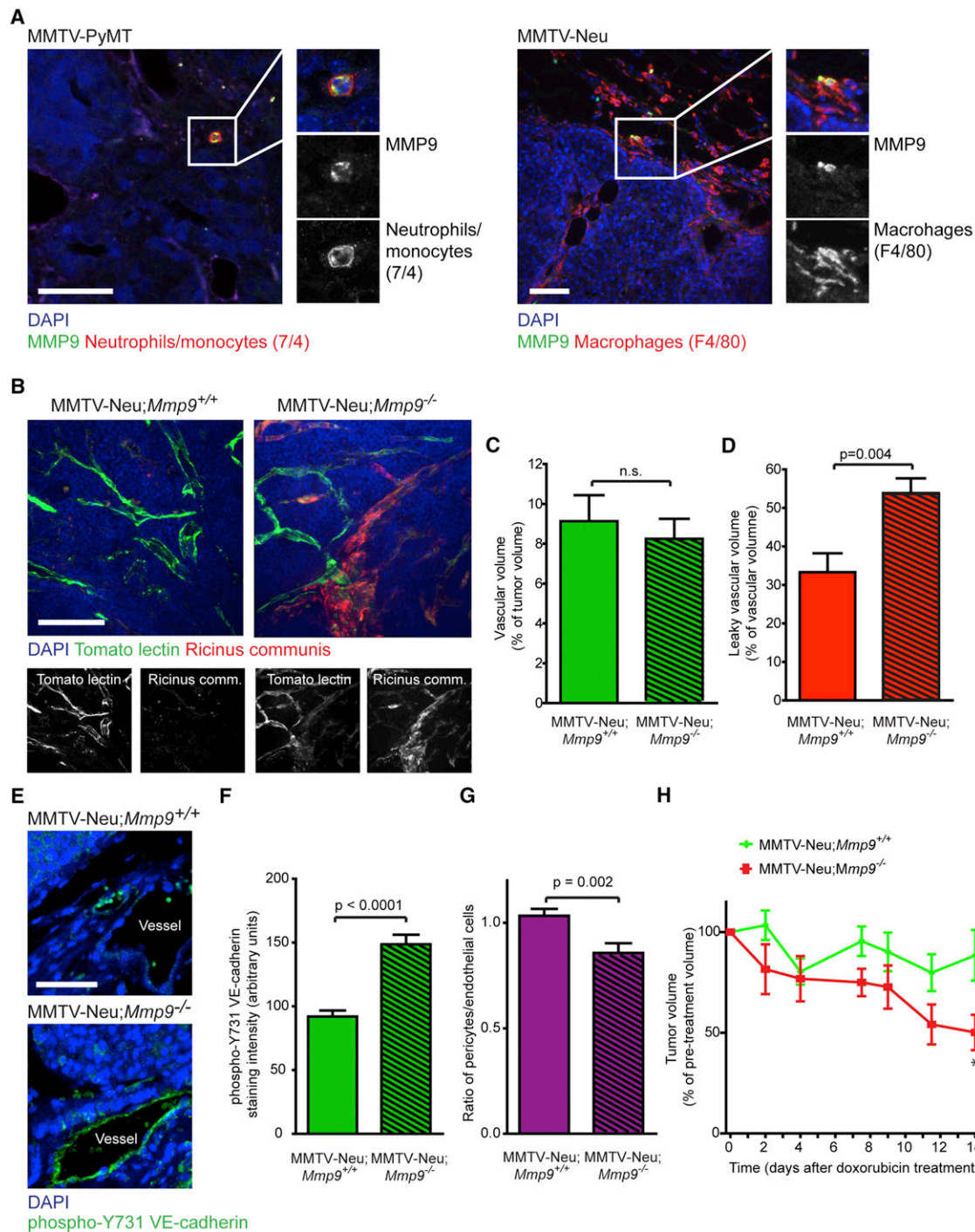


**Figure 5. Matrix Metalloproteinase-9 Is Expressed by Myeloid Cells and Influences Vascular Leakage and Response to Doxorubicin**

(A) MMP9 is expressed by tumor-infiltrating myeloid cells, including those marked by 7/4 (neutrophils/monocytes) and F4/80 (macrophages). Scale bars: 50  $\mu$ m. (B) Vascular structure of tumors in MMTV-Neu;Mmp9<sup>+/+</sup> and MMTV-Neu;Mmp9<sup>-/-</sup> mice analyzed by perfusion with FITC-conjugated tomato lectin (green, labels all blood vessels) and rhodamine-conjugated *Ricinus communis* agglutinin I (red, labels basement membrane exposed to the vascular lumen in leaky vessels). Scale bar: 100  $\mu$ m.

(C) Vascular volume as determined by perfusion with tomato lectin does not differ between MMTV-Neu;Mmp9<sup>+/+</sup> and MMTV-Neu;Mmp9<sup>-/-</sup> mice (mean  $\pm$  SEM, n.s., Student's t test, 33 FOV in ten tumors from five MMTV-Neu;Mmp9<sup>+/+</sup> mice and 29 FOV in eight tumors from three MMTV-Neu;Mmp9<sup>-/-</sup> mice were analyzed).

(D) Blood vessels are leakier in MMTV-Neu;Mmp9<sup>-/-</sup> tumors. The percentage of the vasculature that is positive for *Ricinus communis* agglutinin I shown (mean  $\pm$  SEM, p = 0.004, Student's t test, 33 FOV in ten tumors from five MMTV-Neu;Mmp9<sup>+/+</sup> mice and 29 FOV in eight tumors from three MMTV-Neu;Mmp9<sup>-/-</sup> mice were analyzed).

(E) Immunostaining for phospho-Y731 VE-cadherin. Scale bar: 100  $\mu$ m.

### The Role of Myeloid Cell Recruitment in Chemotherapy Responses

Recruitment of CCR2<sup>+</sup> monocytes after doxorubicin treatment correlated with tumor relapse. Similarly, an increased number of macrophages is found after treatment of tumors with chemotherapy and is associated with poor drug response (Denardo et al., 2011; Shree et al., 2011). Such macrophages can promote cancer cell survival through the secretion of cysteine cathepsins (Shree et al., 2011). CCR2<sup>+</sup> monocytes could be the source of tumor-associated macrophages in the posttreatment micro-environment. Indeed, we did not observe increased numbers of macrophages 48 hr after treatment, whereas they have been observed 7–12 days after the first dose of chemotherapy in the MMTV-PyMT model (Denardo et al., 2011; Shree et al., 2011). However, macrophage infiltration depends on CSF-1 (Denardo et al., 2011). Furthermore, macrophages do not promote survival of cancer cells in a cathepsin-dependent manner after treatment with the cisplatin-related drug carboplatin (Shree et al., 2011), whereas the response to cisplatin was better in *Ccr2*<sup>-/-</sup> hosts. Thus, it is possible that CCR2<sup>+</sup> monocytes and tumor-associated macrophages are recruited through independent pathways and influence drug responses through independent mechanisms. Several such mechanisms likely exist. For example, Tie-2-expressing macrophages are recruited after hypoxic tissue injury through a CXCL12/CXCR4 chemokine axis (Welford et al., 2011).

Our results, as well as those of others (Ahn et al., 2010; Denardo et al., 2011; Shree et al., 2011; Welford et al., 2011), indicate that the myeloid cell infiltration that occurs after chemotherapy, radiation, or tissue injury impedes the response to therapy. However, myeloid cell recruitment can also lead to the direct killing of cancer cells (Guerriero et al., 2011), thereby increasing the response to chemotherapy. These differences in the effects of recruited myeloid cells are likely due to the recruitment of different subpopulations of myeloid cells. Indeed, infiltration of CD206<sup>+</sup> macrophages was associated with increased vascular leakage and better doxorubicin response, whereas reduced CCR2-dependent recruitment of monocytic cells was associated with delayed tumor relapse.

Interestingly, stromal cells expressed CCL2 after doxorubicin treatment. This offers a possible explanation for the observation that stromally derived, but not cancer cell-derived, CCL2 is associated with decreased relapse-free survival in breast cancer patients (Fujimoto et al., 2009). Furthermore, administration of antibodies specific for mouse CCL2 enhances the response to docetaxol in a xenograft model of prostate cancer (Loberg et al., 2007).

### Conclusions

In vivo imaging of tumors shows that different components of the micro-environment participate in the development of

chemoresistance. Disruption of these micro-environments is beneficial for the response to doxorubicin and cisplatin. Our data suggest that existing drugs that inhibit MMPs or chemokine signaling may be effective when combined with traditional chemotherapies. However, the order and timing of administration of such combination therapies could be critical because of the complexity of the interactions between myeloid cells and vasculature in chemotherapy responses. Future studies combining imaging with molecular approaches hold promise for gaining further insights into the targeting of tumors in the context of its micro-environment.

### EXPERIMENTAL PROCEDURES

#### Animals

MMTV-PyMT (FVB/n), MMTV-Neu (FVB/n), ACTB-EGFP (FVB/n), ACTB-H2B-EGFP (obtained on mixed background and backcrossed to FVB/n for six generations), and *Ccr2*<sup>-/-</sup> (C57BL/6) mice were from Jackson Laboratory. MMTV-PyMT (C57BL/6) mice were provided by Dr. Kasper Almholt, and c-fms-EGFP mice were provided by Dr. Jeffrey Pollard and backcrossed to FVB/n mice for six generations. *Mmp9*<sup>-/-</sup> mice (FVB/n) were previously described (Vu et al., 1998). All animal experiments were conducted in accordance with procedures approved by the IACUC at Cold Spring Harbor Laboratory or the University of California, San Francisco.

#### Tumor Transplantation Experiments

Virgin females of 6–16 weeks of age were used as hosts for transplantation. Cancer cells were isolated from 2–3 tumors at 8–10 mm diameter from MMTV-PyMT mice. Tumors were mechanically dissociated and digested with collagenase (0.2% w/v), trypsin (0.2% w/v), and DNase I (8 U/ml) in RPMI-1640 medium. Single cells and debris were removed from the resulting carcinoma organoid preparation by differential centrifugation. Purified carcinoma organoids were dissociated into single cell suspension in 0.25% trypsin with 0.1% ethylene diaminetetraacetic acid and washed in PBS. Cells ( $4 \times 10^5$  in 20  $\mu$ l PBS) were injected into the inguinal mammary glands of host mice.

#### Tumor Response to Doxorubicin and Cisplatin

Mice received 8 mg/kg doxorubicin hydrochloride (in PBS; Sigma-Aldrich, St. Louis, MO, USA) or 10 mg/kg cisplatin (in 10% dimethyl sulfoxide in PBS; MBL International, Woburn, MA, USA) i.p. on days 0, 7, and 14. Control mice were injected with sterile PBS. Tumors were measured 2–3 times a week by caliper, and tumor volumes were calculated as length  $\times$  width<sup>2</sup>/2.

#### Spinning Disk Confocal Imaging of Live Mice

Details of the microscope design and imaging procedure were previously described (Egeblad et al., 2008). To track cell death, mice were injected i.p. with 50  $\mu$ l/h propidium iodide (PI; 0.05–0.1 mg/ml; Invitrogen, Grand Island, NY, USA) in sterile PBS. To determine doxorubicin distribution, MMTV-PyMT mice were injected i.v. with AngioSPARK 680 (100  $\mu$ l of stock solution; VisEn Medical, Waltham, MA, USA) and doxorubicin (8 mg/kg body weight in 200  $\mu$ l PBS). To determine vascular leakage, mice were injected i.v. with 100  $\mu$ l sterile PBS containing 1 mg/ml 10 kD Alexa-Fluor-647-conjugated dextran and 1 mg/ml 2 MD rhodamine-conjugated dextran (Invitrogen).

(F) Depletion of MMP9 increases phosphorylation of VE-cadherin in endothelial cells (mean  $\pm$  SEM,  $p < 0.0001$ , Student's *t* test, 113 vessels from tumors of nine MMTV-Neu;*Mmp9*<sup>+/+</sup> mice and 101 vessels from tumors of nine MMTV-Neu;*Mmp9*<sup>-/-</sup> mice were examined).

(G) Pericyte coverage is decreased in the absence of MMP9. Double immunofluorescence was used to determine the ratio of  $\alpha$ SMA-positive pericytes to CD31-positive endothelial cells (mean  $\pm$  SEM,  $p = 0.002$ , Student's *t* test, 87 vessels from tumors of ten MMTV-Neu;*Mmp9*<sup>+/+</sup> mice and 71 vessels from tumors of nine MMTV-Neu;*Mmp9*<sup>-/-</sup> mice were examined).

(H) MMTV-Neu;*Mmp9*<sup>-/-</sup> ( $n = 7$  tumors from five mice) tumors respond better to treatment with doxorubicin than do MMTV-Neu;*Mmp9*<sup>+/+</sup> tumors ( $n = 11$  tumors from six mice; mean  $\pm$  SEM, \* indicates  $p < 0.05$ ; Student's *t* test). Tumors below 256 mm<sup>3</sup> at the beginning of treatment were excluded from the analysis.

Also see Figure S4.

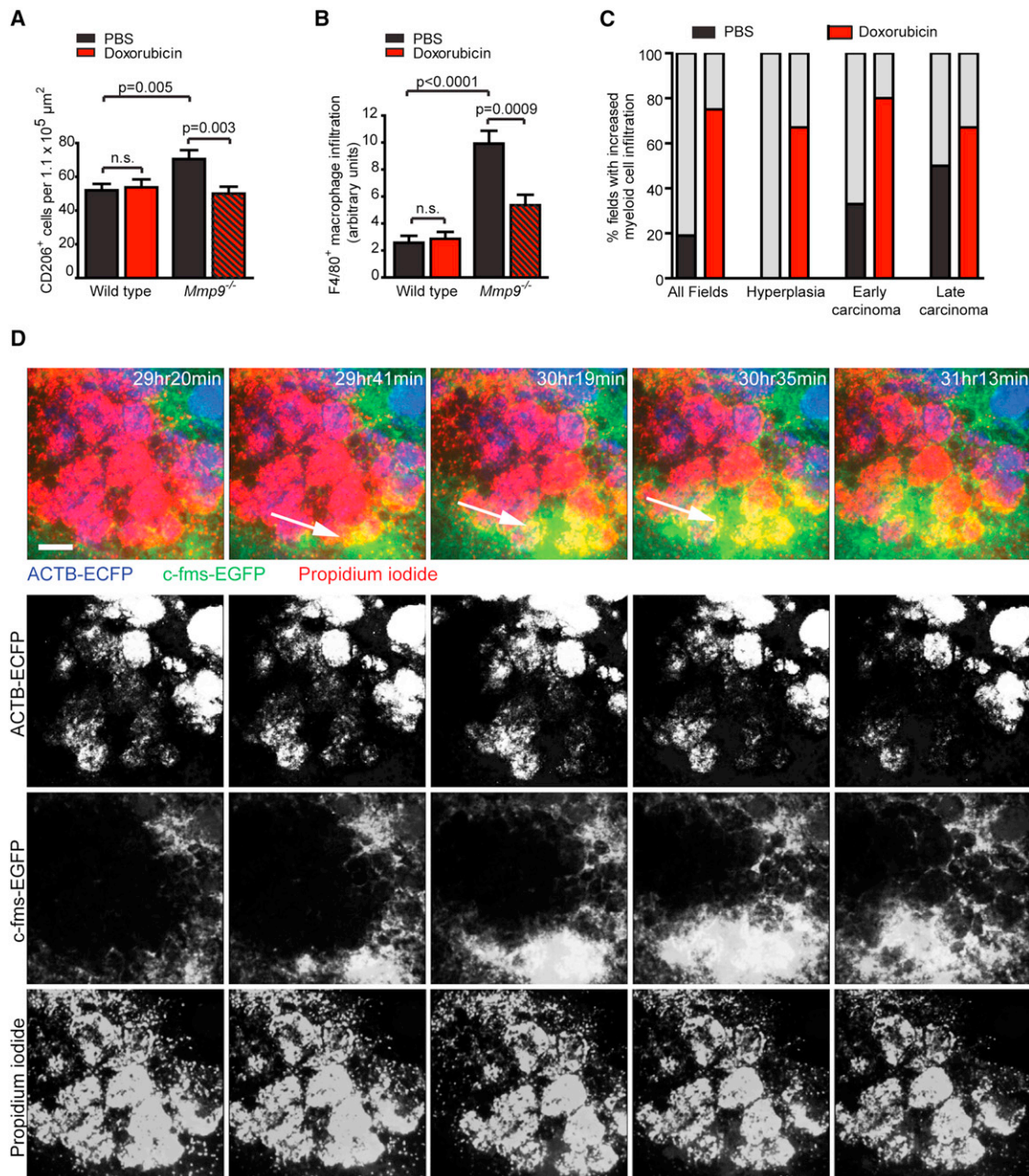


**Figure 6. Myeloid Cells Are Recruited to Areas of Tumor Necrosis**

(A and B) The infiltration of (A) alternatively activated macrophages ( $n = 40$  FOV from tumors of four mice per condition) and (B) the total macrophage population ( $n = 22$ – $30$  FOV from 4–5 mice per condition) is increased in *Mmp9*<sup>-/-</sup> host mice transplanted with MMTV-PyMT tumor cells. The infiltration of these cells decreases 48 hr after doxorubicin treatment (mean  $\pm$  SEM, n.s. or significant as indicated, Student's *t* test).

(C) Myeloid cells are recruited to tumors after doxorubicin treatment (12 of 16 movies) as compared to tumors of PBS-treated control mice (3 of 16 movies,  $p = 0.004$ , Fisher's exact test; three mice were analyzed per condition).

(D) Dynamics of myeloid cell infiltration (arrow) into an area of necrosis in a doxorubicin-treated MMTV-PyMT;ACTB-ECFP;c-fms-EGFP mouse. Time after treatment is indicated. Scale bar: 100  $\mu$ m.

Also see Figure S5 and Movies S7, S8, and S9.

#### Histology and Immunostaining

Paraformaldehyde-fixed, paraffin-embedded sections were stained with Mayer's hematoxylin and eosin. Immunostaining was done with primary antibodies against 7/4 (Cedarlane, Burlington, NC, USA), BrdU and MECA-32 (Developmental Studies Hybridoma Bank, University of Iowa, Iowa City,

IA, USA), CCL2, CD206, and F4/80 (AbD Serotec, Raleigh, NC, USA), CCR2 (Novus Biologicals, Littleton, CO, USA), phospho-histone H2AX and phospho-histone H3 (Cell Signaling, Danvers, MA, USA),  $\alpha$ SMA (Sigma-Aldrich), CD31 and phospho-VE-cadherin (Abcam, Cambridge, MA, USA), and MMP9 (Rasch et al., 2010). Immunostained slides were quantified by counting

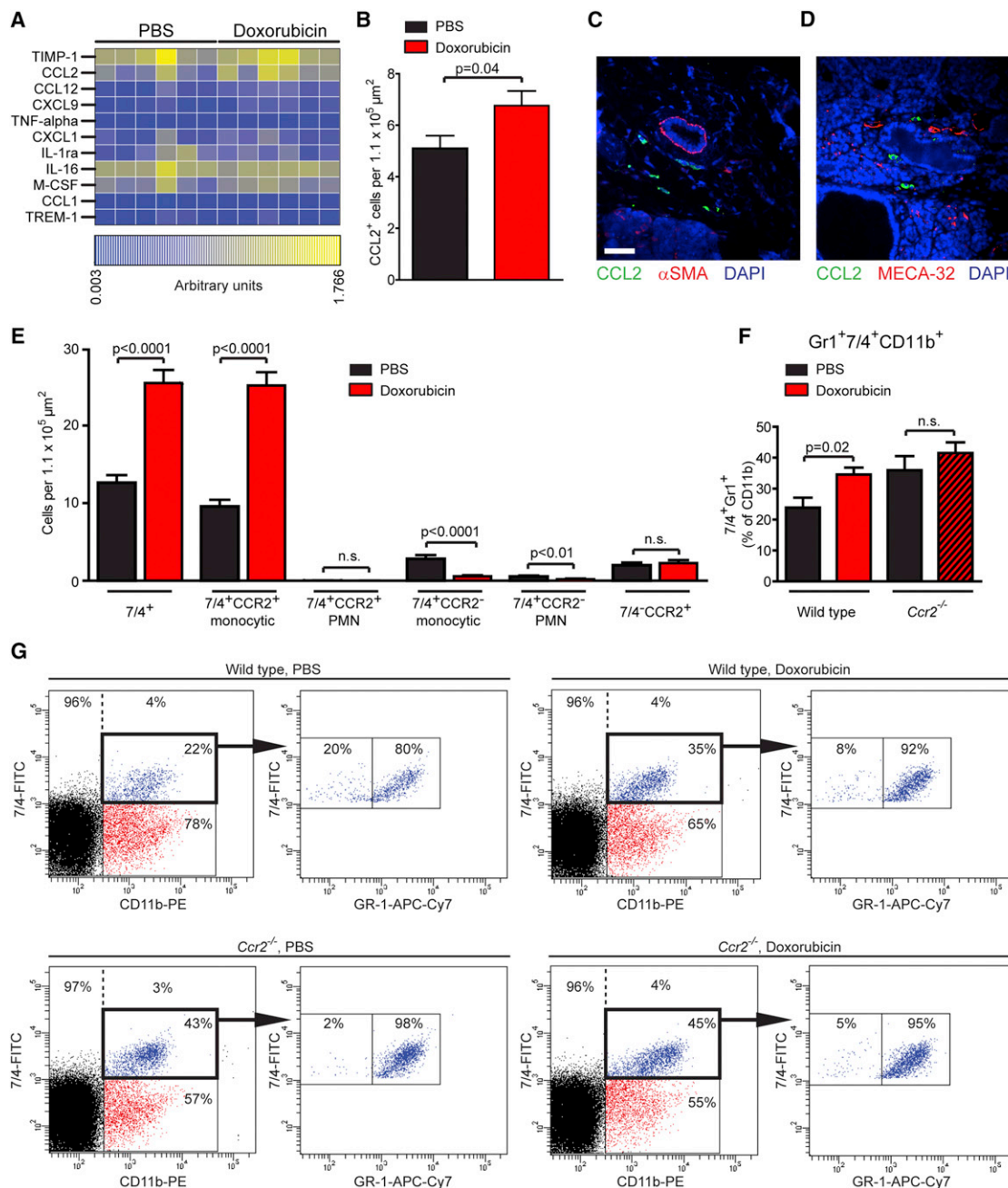


**Figure 7. Myeloid Cells Are Recruited to Doxorubicin-treated Tumors through a Stromal CCL2/CCR2 Chemokine/Chemokine Receptor Axis**  
(A) Protein array identifies CCL2 as the most upregulated chemokine in tumor lysates 48 hr after doxorubicin treatment (p = 0.09 for CCL2 and p = 0.03 for CCL12, Student's t test). Each column represents a tumor from a different mouse.  
(B) The number of CCL2-expressing cells increases 48 hr after treatment with doxorubicin (mean ± SEM, p = 0.04, Student's t test; 80 FOV from six PBS-treated and 66 FOV from six doxorubicin-treated mice were analyzed).  
(C and D) Endothelial cells, pericytes, and fibroblasts do not express CCL2. Tumor tissue from MTMV-PyMT mice isolated 48 hr after treatment with doxorubicin was immunostained for CCL2 and (C) α-smooth muscle actin (αSMA, a pericyte, and fibroblast marker) or (D) MECA-32 (an endothelial cell marker). More than 300 αSMA or MECA-32 positive cells from PBS and doxorubicin-treated tumors were observed, and none were positive for CCL2. Scale bar: 50 μm.  
(E) Doxorubicin treatment results in infiltration of 7/4<sup>+</sup>CCR2<sup>+</sup> cells with monocytic but not polymorphonuclear (PMN) morphology. Double immunostaining for CCR2 and 7/4 with scoring of nuclear morphology (mean ± SEM, Student's t test, significance levels as indicated; 104 FOV from four PBS-treated and 113 FOV from five doxorubicin-treated mice).  
(F) Doxorubicin results in CCR2-dependent myeloid cell infiltration. The percentage of Gr1<sup>+</sup>7/4<sup>+</sup> of all CD11b<sup>+</sup> myeloid cells in tumors was determined by flow cytometry (mean ± SEM, significance levels as indicated, Student's t test, n = 10–11 mice).  
(G) FACS plots with indication of the percentages of the gated cell populations from representative tumors.  
Also see Figure S6.

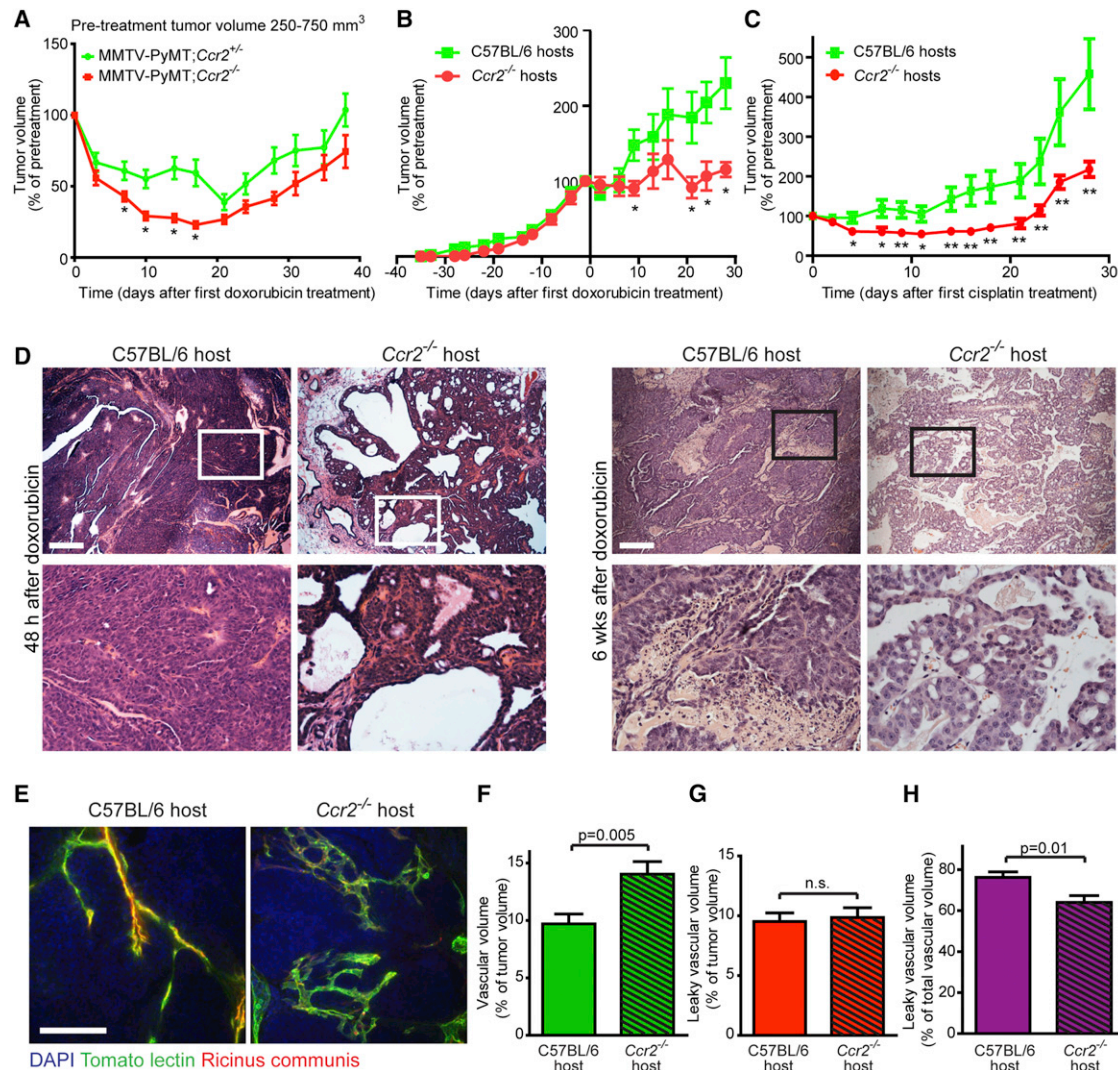


**Figure 8. Host CCR2 Regulates Response to Doxorubicin**

(A) Tumors in MMTV-PyMT;*Ccr2*<sup>-/-</sup> (26 tumors from ten mice) respond better to doxorubicin than those in MMTV-PyMT;*Ccr2*<sup>+/+</sup> (15 tumors from eight mice). Results for tumors with a pretreatment volume of 250–750 mm<sup>3</sup> (mean ± SEM, \* indicates p < 0.05, Student's t test).

(B) Tumors in *Ccr2*<sup>-/-</sup> host mice respond better to doxorubicin than those in *C57BL/6* hosts. Two cohorts were treated with doxorubicin and showed similar results. The results of one cohort are shown (mean ± SEM, \* indicates p < 0.05, Student's t test; eight tumors in 6–8 hosts were analyzed per condition; one *Ccr2*<sup>-/-</sup> and two *C57BL/6* hosts were euthanized on days 13–16 due to poor health).

(C) Tumors in *Ccr2*<sup>-/-</sup> hosts respond better to cisplatin than those in *C57BL/6* hosts (mean ± SEM, \* indicates p < 0.05, \*\* indicates p < 0.01, Student's t test, n = 22–24 tumors in 11–12 hosts).

(D) Tumors in *Ccr2*<sup>-/-</sup> hosts are more cystic and contain fewer cancer cells acutely (48 hr) after doxorubicin treatment. Relapsed tumors (six weeks after treatment) in *Ccr2*<sup>-/-</sup> hosts are low-grade with decreased cellularity and necrosis (p = 0.005, Fisher's exact test; ten low-grade and five high-grade tumors in *Ccr2*<sup>-/-</sup> hosts versus one low-grade and eleven high-grade tumors in *C57BL/6* hosts). Scale bar: 100 μm.

(E) Vascular structure of tumors in *Ccr2*<sup>-/-</sup> and *C57BL/6* hosts analyzed by perfusion with FITC-conjugated tomato lectin (green) and rhodamine-conjugated *Ricinus communis* agglutinin I (red). Nuclei are stained with 4',6-diamidino-2-phenylindole. Scale bar: 100 μm.

(F) Vascular volume is increased in tumors in *Ccr2*<sup>-/-</sup> hosts compared to *C57BL/6* wild-type hosts as determined by perfusion with tomato lectin (mean ± SEM, p = 0.005, Student's t test; analysis of 12 tumors from six mice per genotype and 5–10 fields of view per tumor).

(G) The total volume of leaky vasculature does not differ between tumors in *Ccr2*<sup>-/-</sup> and *C57BL/6* hosts (mean ± SEM; n.s., Student's t test; analysis of 12 tumors from six mice per genotype and 5–10 FOV per tumor).

(H) Relative leaky vasculature is decreased in tumors of *Ccr2*<sup>-/-</sup> hosts compared to *C57BL/6* hosts as determined by the percentage of the vasculature that is positive for *Ricinus communis* agglutinin I (mean ± SEM, p = 0.01, Student's t test; analysis of 12 tumors from six mice per genotype and 5–10 FOV per tumor). Also see Figure S7.

(for 7/4, BrdU, CCL2, CCR2, CD206, phospho-histone H2AX, and phospho-histone H3) or by fluorescence intensity with Volocity software (PerkinElmer; for F4/80, phospho-VE-cadherin, αSMA, and CD31).

#### In Vitro Drug Sensitivity

Tumor lesions were isolated from MMTV-PyMT;ACTB-ECFP mice using a fluorescent dissection microscope, and primary mammary organoids were

isolated from different tumor stages and cultured in Growth Factor Reduced Matrigel (BD Biosciences, San Diego, CA, USA). To determine doxorubicin sensitivity, treatment of tumor organoids was started 72 hr after isolation. To determine lapatinib sensitivity, single cell suspensions were generated from tumor organoids, isolated as described previously, grown to subconfluence, re-seeded, and treated with lapatinib (Selleck Chemicals, LLC, Houston, TX, USA). Cell viability was measured 48 hr after the addition of drugs using the CellTiter 96 Aqueous One Solution Cell Proliferation Assay (Promega, Madison, WI, USA).

For further experimental details, see [Supplemental Experimental Procedures](#).

## SUPPLEMENTAL INFORMATION

Supplemental Information includes seven figures, nine movies, and Supplemental Experimental Procedures and can be found with this article online at [doi:10.1016/j.ccr.2012.02.017](http://doi:10.1016/j.ccr.2012.02.017).

## ACKNOWLEDGMENTS

We thank E. Atamaniuc, Y. Yu, H. Capili, J. Cappellani, G. DiMino, M.B. Ebert, J. Waage, J. Paterek, and the Shared Resources at CSHL for technical support. Dr. Claire Lewis is thanked for helpful comments on the manuscript. Antibodies against BrdU and MECA-32 were obtained from the Developmental Studies Hybridoma Bank maintained by the University of Iowa. This work was supported by funds from the National Cancer Institute (U01 CA141451 to M.E.; R01 CA057621 to Z.W. and M.J.B.; and P50 CA088843 to A.J.E.), the Starr Cancer Consortium, the Breast Cancer Alliance, Susan G. Komen for the Cure, Long Island 2 Day Walk to Fight Breast Cancer and Manhasset Women's Coalition Against Breast Cancer to M.E., the Stand Up to Cancer-American Association for Cancer Research Dream Team Translational Cancer Research Grant (SU2C-AACR-DT0409 to Z.W.), a predoctoral fellowship from the Congressionally Directed Breast Cancer Research Program, U.S. (E.S.N.), the Research Council of Norway (160698/V40 and 151882 [FUGE] to E.F.), and Southeastern Regional Health Authorities (2007060 to E.F.). E.S.N. is the recipient of the Leslie C. Quick and William Randolph Hearst Foundation Fellowships from the Watson School of Biological Sciences. E.F. and H.A.A. were supported by "University of Oslo Research Fund (UNIFOR)" and Ullevål University Hospital Research Fund (VIRUUS).

Received: May 4, 2011

Revised: December 18, 2011

Accepted: February 17, 2012

Published: April 16, 2012

## REFERENCES

Ahn, G.O., Tseng, D., Liao, C.H., Dorie, M.J., Czechowicz, A., and Brown, J.M. (2010). Inhibition of Mac-1 (CD11b/CD18) enhances tumor response to radiation by reducing myeloid cell recruitment. *Proc. Natl. Acad. Sci. USA* **107**, 8363–8368.

Campiglio, M., Somenzi, G., Oliati, C., Beretta, G., Balsari, A., Zaffaroni, N., Valagussa, P., and Ménard, S. (2003). Role of proliferation in HER2 status predicted response to doxorubicin. *Int. J. Cancer* **105**, 568–573.

Coussens, L.M., Fingleton, B., and Matrisian, L.M. (2002). Matrix metalloproteinase inhibitors and cancer: trials and tribulations. *Science* **295**, 2387–2392.

Dean, M., Fojo, T., and Bates, S. (2005). Tumour stem cells and drug resistance. *Nat. Rev. Cancer* **5**, 275–284.

Denardo, D.G., Brennan, D.J., Rexhepaj, E., Ruffell, B., Shiao, S.L., Madden, S.F., Gallagher, W.M., Wadhwani, N., Keil, S.D., Junaid, S.A., et al. (2011). Leukocyte complexity predicts breast cancer survival and functionally regulates response to chemotherapy. *Cancer Discov.* **1**, 54–67.

Dive, C., Gregory, C.D., Phipps, D.J., Evans, D.L., Milner, A.E., and Wyllie, A.H. (1992). Analysis and discrimination of necrosis and apoptosis (programmed cell death) by multiparameter flow cytometry. *Biochim. Biophys. Acta* **1133**, 275–285.

Ebrahem, Q., Chaurasia, S.S., Vasanji, A., Qi, J.H., Klenotic, P.A., Cutler, A., Asosingh, K., Erzurum, S., and Anand-Apte, B. (2010). Cross-talk between vascular endothelial growth factor and matrix metalloproteinases in the induction of neovascularization in vivo. *Am. J. Pathol.* **176**, 496–503.

Egeblad, M., Ewald, A.J., Askautrud, H.A., Truitt, M.L., Welm, B.E., Bainbridge, E., Peeters, G., Krummel, M.F., and Werb, Z. (2008). Visualizing stromal cell dynamics in different tumor microenvironments by spinning disk confocal microscopy. *Dis. Model Mech.* **1**, 155–167.

Egeblad, M., Nakasone, E.S., and Werb, Z. (2010). Tumors as organs: complex tissues that interface with the entire organism. *Dev. Cell* **18**, 884–901.

Fujimoto, H., Sangai, T., Ishii, G., Ikehara, A., Nagashima, T., Miyazaki, M., and Ochiai, A. (2009). Stromal MCP-1 in mammary tumors induces tumor-associated macrophage infiltration and contributes to tumor progression. *Int. J. Cancer* **125**, 1276–1284.

Gavard, J. (2009). Breaking the VE-cadherin bonds. *FEBS Lett.* **583**, 1–6.

Gilbert, L.A., and Hemann, M.T. (2010). DNA damage-mediated induction of a chemoresistant niche. *Cell* **143**, 355–366.

Goel, S., Duda, D.G., Xu, L., Munn, L.L., Boucher, Y., Fukumura, D., and Jain, R.K. (2011). Normalization of the vasculature for treatment of cancer and other diseases. *Physiol. Rev.* **91**, 1071–1121.

Gong, Y., Hart, E., Shchurin, A., and Hoover-Plow, J. (2008). Inflammatory macrophage migration requires MMP-9 activation by plasminogen in mice. *J. Clin. Invest.* **118**, 3012–3024.

Greene, R.F., Collins, J.M., Jenkins, J.F., Speyer, J.L., and Myers, C.E. (1983). Plasma pharmacokinetics of adriamycin and adriamycinol: implications for the design of in vitro experiments and treatment protocols. *Cancer Res.* **43**, 3417–3421.

Guerriero, J.L., Ditsworth, D., Catanzaro, J.M., Sabino, G., Furie, M.B., Kew, R.R., Crawford, H.C., and Zong, W.X. (2011). DNA alkylating therapy induces tumor regression through an HMGB1-mediated activation of innate immunity. *J. Immunol.* **186**, 3517–3526.

Hadjantonakis, A.K., and Papaioannou, V.E. (2004). Dynamic in vivo imaging and cell tracking using a histone fluorescent protein fusion in mice. *BMC Biotechnol.* **4**, 33.

Hagendoorn, J., Tong, R., Fukumura, D., Lin, Q., Lobo, J., Padera, T.P., Xu, L., Kuchelapati, R., and Jain, R.K. (2006). Onset of abnormal blood and lymphatic vessel function and interstitial hypertension in early stages of carcinogenesis. *Cancer Res.* **66**, 3360–3364.

Herschkowitz, J.I., Simin, K., Weigman, V.J., Mikaelian, I., Usary, J., Hu, Z., Rasmussen, K.E., Jones, L.P., Assefnia, S., Chandrasekharan, S., et al. (2007). Identification of conserved gene expression features between murine mammary carcinoma models and human breast tumors. *Genome Biol.* **8**, R76.

Johnson, J.I., Decker, S., Zaharevitz, D., Rubinstein, L.V., Venditti, J.M., Schepartz, S., Kalyandrug, S., Christian, M., Arbuck, S., Hollingshead, M., and Sausville, E.A. (2001). Relationships between drug activity in NCI preclinical in vitro and in vivo models and early clinical trials. *Br. J. Cancer* **84**, 1424–1431.

Lin, E.Y., Jones, J.G., Li, P., Zhu, L., Whitney, K.D., Muller, W.J., and Pollard, J.W. (2003). Progression to malignancy in the polyoma middle T oncoprotein mouse breast cancer model provides a reliable model for human diseases. *Am. J. Pathol.* **163**, 2113–2126.

Loberg, R.D., Ying, C., Craig, M., Day, L.L., Sargent, E., Neeley, C., Wojno, K., Snyder, L.A., Yan, L., and Pienta, K.J. (2007). Targeting CCL2 with systemic delivery of neutralizing antibodies induces prostate cancer tumor regression in vivo. *Cancer Res.* **67**, 9417–9424.

Loeffler, M., Krüger, J.A., Niethammer, A.G., and Reisfeld, R.A. (2006). Targeting tumor-associated fibroblasts improves cancer chemotherapy by increasing intratumoral drug uptake. *J. Clin. Invest.* **116**, 1955–1962.

Martin, M.D., Carter, K.J., Jean-Philippe, S.R., Chang, M., Mobashery, S., Thiolloy, S., Lynch, C.C., Matrisian, L.M., and Fingleton, B. (2008). Effect of ablation or inhibition of stromal matrix metalloproteinase-9 on lung metastasis in a breast cancer model is dependent on genetic background. *Cancer Res.* **68**, 6251–6259.

- Meads, M.B., Gatenby, R.A., and Dalton, W.S. (2009). Environment-mediated drug resistance: a major contributor to minimal residual disease. *Nat. Rev. Cancer* 9, 665–674.
- Minchinton, A.I., and Tannock, I.F. (2006). Drug penetration in solid tumours. *Nat. Rev. Cancer* 6, 583–592.
- Murdoch, C., Giannoudis, A., and Lewis, C.E. (2004). Mechanisms regulating the recruitment of macrophages into hypoxic areas of tumors and other ischemic tissues. *Blood* 104, 2224–2234.
- Netti, P.A., Hamberg, L.M., Babich, J.W., Kierstead, D., Graham, W., Hunter, G.J., Wolf, G.L., Fischman, A., Boucher, Y., and Jain, R.K. (1999). Enhancement of fluid filtration across tumor vessels: implication for delivery of macromolecules. *Proc. Natl. Acad. Sci. USA* 96, 3137–3142.
- Obeid, M., Tesniere, A., Ghiringhelli, F., Fimia, G.M., Apetoh, L., Perfettini, J.L., Castedo, M., Mignot, G., Panaretakis, T., Casares, N., et al. (2007). Calreticulin exposure dictates the immunogenicity of cancer cell death. *Nat. Med.* 13, 54–61.
- Olive, K.P., Jacobetz, M.A., Davidson, C.J., Gopinathan, A., McIntyre, D., Honess, D., Madhu, B., Goldgraben, M.A., Caldwell, M.E., Allard, D., et al. (2009). Inhibition of Hedgehog signaling enhances delivery of chemotherapy in a mouse model of pancreatic cancer. *Science* 324, 1457–1461.
- Pahler, J.C., Tazzyman, S., Erez, N., Chen, Y.Y., Murdoch, C., Nozawa, H., Lewis, C.E., and Hanahan, D. (2008). Plasticity in tumor-promoting inflammation: impairment of macrophage recruitment evokes a compensatory neutrophil response. *Neoplasia* 10, 329–340.
- Priceman, S.J., Sung, J.L., Shaposhnik, Z., Burton, J.B., Torres-Collado, A.X., Moughon, D.L., Johnson, M., Lusa, A.J., Cohen, D.A., Iruela-Arispe, M.L., and Wu, L. (2010). Targeting distinct tumor-infiltrating myeloid cells by inhibiting CSF-1 receptor: combating tumor evasion of antiangiogenic therapy. *Blood* 115, 1461–1471.
- Rasch, M.G., Lund, I.K., Illemann, M., Hoyer-Hansen, G., and Gårdsvoll, H. (2010). Purification and characterization of recombinant full-length and protease domain of murine MMP-9 expressed in *Drosophila* S2 cells. *Protein Expr. Purif.* 72, 87–94.
- Rottenberg, S., Pajic, M., and Jonkers, J. (2010). Studying drug resistance using genetically engineered mouse models for breast cancer. *Methods Mol. Biol.* 596, 33–45.
- Rouzier, R., Perou, C.M., Symmans, W.F., Ibrahim, N., Cristofanilli, M., Anderson, K., Hess, K.R., Stec, J., Ayers, M., Wagner, P., et al. (2005). Breast cancer molecular subtypes respond differently to preoperative chemotherapy. *Clin. Cancer Res.* 11, 5678–5685.
- Sadik, C.D., Kim, N.D., and Luster, A.D. (2011). Neutrophils cascading their way to inflammation. *Trends Immunol.* 32, 452–460.
- Shree, T., Olson, O.C., Elie, B.T., Kester, J.C., Garfall, A.L., Simpson, K., Bell-McGuinn, K.M., Zabor, E.C., Brogi, E., and Joyce, J.A. (2011). Macrophages and cathepsin proteases blunt chemotherapeutic response in breast cancer. *Genes Dev.* 25, 2465–2479.
- Sounni, N.E., Dehne, K., van Kempen, L., Egeblad, M., Affara, N.I., Cuevas, I., Wiesen, J., Junankar, S., Korets, L., Lee, J., et al. (2010). Stromal regulation of vessel stability by MMP14 and TGFβ. *Dis. Model Mech.* 3, 317–332.
- Thurston, G., Suri, C., Smith, K., McClain, J., Sato, T.N., Yancopoulos, G.D., and McDonald, D.M. (1999). Leakage-resistant blood vessels in mice transgenically overexpressing angiopoietin-1. *Science* 286, 2511–2514.
- Tsou, C.L., Peters, W., Si, Y., Slaymaker, S., Aslanian, A.M., Weisberg, S.P., Mack, M., and Charo, I.F. (2007). Critical roles for CCR2 and MCP-3 in monocyte mobilization from bone marrow and recruitment to inflammatory sites. *J. Clin. Invest.* 117, 902–909.
- Vu, T.H., Shipley, J.M., Bergers, G., Berger, J.E., Helms, J.A., Hanahan, D., Shapiro, S.D., Senior, R.M., and Werb, Z. (1998). MMP-9/gelatinase B is a key regulator of growth plate angiogenesis and apoptosis of hypertrophic chondrocytes. *Cell* 93, 411–422.
- Welford, A.F., Biziato, D., Coffelt, S.B., Nucera, S., Fisher, M., Pucci, F., Di Serio, C., Naldini, L., De Palma, M., Tozer, G.M., and Lewis, C.E. (2011). TIE2-expressing macrophages limit the therapeutic efficacy of the vascular-disrupting agent combretastatin A4 phosphate in mice. *J. Clin. Invest.* 121, 1969–1973.
- Yu, Q., and Stamenkovic, I. (2000). Cell surface-localized matrix metalloproteinase-9 proteolytically activates TGF-β and promotes tumor invasion and angiogenesis. *Genes Dev.* 14, 163–176.
- Zhang, J., Lu, Y., and Pienta, K.J. (2010). Multiple roles of chemokine (C-C motif) ligand 2 in promoting prostate cancer growth. *J. Natl. Cancer Inst.* 102, 522–528.